Escola de Camins
Escola Tècnica Superior d'Enginyeria de Camins, Canals i Ports
UPC BARCELONATECH

# MASTER THESIS

## Master

**Civil and Environmental Engineering**

## Title

**Shear strength of beams with loads close to supports**

## Author

**Sebastian Webb**

## Tutor

**Prof. Antonio Marí**

## Speciality

**Structural Engineering**

## Date

**8/5/2015**

## Abstract

In reinforced concrete beams subjected to concentrated loads, the shear resisted increases considerably as the loads approach to the support. There is not a consensus in the current codes of practice about any simple design formulation which adequately considers this phenomenon.

A mechanical model has been developed at the Polytechnic University of Barcelona, which predicts the shear strength of beams. The model is originally applicable to slender beams (a/d >2.0-2.5), and is under consideration for adoption into the Eurocodes. The model deals with shear-flexure failure, in which flexural cracks develop inclined through the web and stabilized near the neutral axis. Failure is assumed to happen when this flexural crack develops inside the compression chord, subjected to normal and shear stresses, which takes place when the stresses reach the biaxial failure envelope of Kupfer.

The model has been extended to cases where the loads are applied near the supports. In this case, the Bernoulli assumption (Plane sections remain plane) is no longer valid, and the problem must be faced as a typical discontinuity “D” region, because the dimensions (a/d<2) and because the vertical stresses introduced by the vertical loads by means of the bearing plates interact with the state of stresses of the compression chord.

The extension of the model proposed at UPC consists on incrementing the neutral axis depth as the load approaches the supports and including the vertical stresses due to the applied concentrated loads, as confinement stresses in the concrete, thus changing the state of principal stress in the failure envelope from tension-compression to compression-compression, thus enhancing the shear capacity

In this thesis, a data base of beams with loads near the supports, with and without stirrups, has been collected. A comparison between the predictions of the proposed model and the predictions of the Eurocodes has been made, using the collected data base of 121 short-span beams which failed in shear. 43 of the beams had stirrups, while the last 78 were not transversally reinforced, all the beams have a/d-ratios of less than 2.5.

The results obtained in this thesis are approximate to the results achieved in other literature. The proposed model compares favourably to the Eurocode for beams with and without shear reinforcement. In addition, some of the assumptions of the new model have been investigated using a 2D finite element model. The results obtained with the 2D FEM confirm the assumptions used in the model.

**Keywords:** Short-span beams, shear, reinforced concrete beams, concrete beams, shear strength, shear failure, shear enhancement.

**Acknowledgements**

This work has been done as part of a Master's degree at the University of Strathclyde, but has been done at the Polytechnic University of Barcelona. If not for the Erasmus exchange program between Strathclyde and UPC and the, this project would not have been possible and I would like to acknowledge both universities and the Erasmus student exchange program.

I would like to thank Noemi Duarte and Raul Menduiña Montero for their guidance and help with the data analysis and the FEM model generation.

The support offered by my supervisor, Prof. Antonio Marí, has been invaluable. I especially would like to thank him for his time, patience, help and supervision.

Contents

## Table of tables



## Table of figures

**Notation**

a: shear span

b: width of concrete section

d: effective depth to main tension reinforcement

$d_{max}$: maximum aggregate size

$f_{cc}$: uniaxial concrete compressive strength

$f_{ck}$: characteristic value of the cylinder concrete compressive strength

$f_{cm}$: mean value of the cylinder concrete compressive strength

$f_{ct}$: uniaxial concrete tensile strength

$f_{ctm}$: mean value of the concrete tensile strength

$f_{yw}$: yield strength of the transverse reinforcement

h: overall depth of concrete section

$l_{sw}$: crack length

$l_w$: length along the crack where the tensile stresses are extended

$n_b$: number of longitudinal bars

s: longitudinal coordinate from the support

$s_{cr}$: location of the section where the critical shear crack starts

$s_{mx}$: average crack spacing of inclined cracks along the beam axis

$s_{m\theta}$: average crack spacing of inclined cracks

$s_t$: stirrups spacing

$s_u$: location of the shear critical section vc: dimensionless contribution to the shear strength of the un-cracked concrete chord

$v_l$: dimensionless contribution to the shear strength of the longitudinal reinforcement

$v_s$: dimensionless contribution to the shear strength of the transverse reinforcement

$v_u$: dimensionless ultimate shear force

$v_{u,0}$: dimensionless ultimate shear force of beams and one-way slabs without transverse reinforcement

$v_w$: dimensionless shear force resisted along the crack

w: crack width

$w_{max}$: maximum crack width

$w_x$: crack opening in the horizontal direction

$w_y$: crack opening in the vertical direction

x: neutral axis depth

$x_w$: vertical projection of lw

y: vertical coordinate from the top fibre of the concrete element

z: lever arm

$A_s$: longitudinal reinforcement area

$A_{sw}$: area per unit length of the transverse reinforcement

C: compression force in the un-cracked concrete chord

$E_c$: modulus of elasticity of concrete

$E_s$: modulus of elasticity of steel

$G_c$: modulus of shear deformation for the un-cracked concrete chord

$G_f$: concrete fracture energy

$I_s$: modulus of inertia of the longitudinal reinforcement bar

$K_\lambda$: constant

M: bending moment

$M_{cr}$: cracking moment

$R_t$: ratio between the principal tensile stress and the tensile strength

S: strut force

T: tensile force in the longitudinal reinforcement

V: shear force

$V_c$: contribution to the shear strength of the un-cracked concrete chord

$V_l$: contribution to the shear strength of the longitudinal reinforcement

$V_{pred}$: predicted value of the ultimate shear force

$V_s$: contribution to the shear strength of the transverse reinforcement

$V_{Sd}$: design shear force

$V_{exp}$: experimental value of the ultimate shear force

$V_u$: ultimate shear force

$V_{u,0}$: ultimate shear force of beams and one-way slabs without transverse reinforcement

$V_w$: shear force resisted along the crack

α: inclination angle of shear reinforcement or ties

$\alpha_e$: modular ratio (Es/Ec)

$\delta_w$: crack opening in the vertical direction

$\delta_v$: crack sliding in the vertical direction

ϕ: diameter of reinforcement bar

$\varepsilon_{ct,cr}$: concrete strain at the beginning of macro-cracking

$\varepsilon_{ct,u}$: ultimate tensile strain

$\varepsilon_s$: strain at the longitudinal reinforcement

$\varepsilon_{sx}$: axial strain at the longitudinal reinforcement

$\varepsilon_{sw}$: tensile strain normal to the crack

$\varepsilon_x$: strain in the longitudinal direction

ζ: size effect factor

γ: distortion

λ: distance from the neutral axis

θ: inclination angle of the strut

μ: dimensionless bending moment (M/( fct·b·d))

$\mu_{cr}$: dimensionless cracking moment (Mcr/( fct·b·d))

ξ: dimensionless neutral axis depth

$\xi_w$: dimensionless vertical projection of lw

ρ: longitudinal tension reinforcement ratio

$\rho_w$: transverse reinforcement ratio

$\sigma_1$, $\sigma_2$: principal stresses

$\sigma_{st}$: stress in the transversal reinforcement

$\sigma_x$: normal stress in the longitudinal direction

$\sigma_{x,max}$: maximum normal stress in the longitudinal direction

$\sigma_y$: normal stress in the transverse direction

$\sigma_w$: normal stress in a horizontal fibre in the cracked web

τ: shear stress

$\tau_{max}$: maximum shear stress

$\tau_\lambda$: shear stress at $y = \lambda \cdot x$

# Chapter 1. Introduction and objectives

## 1.1 Introduction

Shear failure is a complex phenomenon, subject to many factors and resisted by various mechanisms. A large amount of research has been undertaken on the topic the past 60 years and have been summarized by Collins, Bentz and Sherwood (2008) and Reineck, Kuchma, Kim and Marx (2003).

There have been developed theoretical shear failure models (Vecchio & Collins, 1986; Petrangeli, Pinto & Ciampi, 1999), but they have been too complex and time consuming to adapt into design codes. In response to this, simple semi empirical models have been developed and adopted (European Committee for Standardization (CEN), 2002; ACI Committee 318. 2008), but studies have shown (Sagaseta & Vollum, 2011) that EC-2 overestimates or underestimates the shear strength of beams, depending on aggregate type and cross section type.

Because design codes need to cover all possible cases, they need to be conservative. The conservativeness of the design codes depend on the precision and accuracy of the prediction. More precise predictions have less scatter and dispersion. Adoption of models with less scatter makes designs more economical. In addition, it prevents the premature destruction of structures deemed unsafe.

The Tooth model (Reineck, 1991), Simplified Compression Field Theory (Bentz, 2010; Fédération Internationale du Béton,2013), the critical crack theory (Muttoni, 2008; Muttoni & Ruiz, 2008), the splitting test analogy model (Desai, 2004; Zararis 2003; Zararis & Papadakis, 2001) and the theories based on the resistance of the un-cracked concrete compression chord (Choi, Park, & Wight, 2007; Khuntia & Stojadinovic, 2001; Kotsovos, Bobrowski, & Eibl, 1987; Park, Choi, & Wight, 2006; Park, Kang, & Choi, 2013; Ruddle, Rankin, & Long, 1999; Tureyen & Frosch, 2003; Tureyen, Wolf, & Frosch, 2006; Wolf & Frosch, 2007; Zanuy, Albajar, & Gallego, 2011) are models that have attempted to model shear strength of beams. While these models have emphasized different shear strength contributors, they all have well-fitting results. Mari et al. (2014) prosed that the reason that these models fit well, but emphasised different shear strength contributors is that the different contributors act at different stages of loading.

Mari et al. (2014) thus created a mechanical model which incorporates the most important aspects of the different shear models. The models predictions were tested against the database gathered by Collins et al. (2008) and yielded results with lower dispersion than the EC-2. A simplified version of the model is under consideration for adoption into the EC-2.

The purpose of this paper is to extend his work by investigating the accuracy of the model for loads close to support (a/d-ratios >2.5), and compare the predictions of this new proposed model to that of the EC-2 and verify this against a database.

## 1.2 Thesis objective

The objective of this thesis is to gather the relevant data for the proposed theory from 5 research papers (Cossio & Siess, 1960; Kani, 1969, Kani, 1967; Smith & Vantsiotis 1983; Vollum & Fang, 2014) in order to evaluate the accuracy of its predictions. All of the data is of cases where the load is close to the support, which is defined as a/d = 2.5. a is the shear span and d is the effective depth of the beam. The predictions of the proposed theory will be compared to the predictions of other design codes and to the experimental results. For simplicity, beams subject to axial loads were not considered.

Secondly, the FEM software Midas-FEA will be used to investigate the assumptions made in the new model. In order to do this, the vertical stresses in beams subject to loads close to the support will be investigated. It will be a 2D model. The loads will be applied at a/d-ratios equal to 2, 1.5 and 1.

# Chapter 2. Literature review

## 2.2 Shear transfer mechanism

A beam that fails in shear will develop a diagonal crack similar to that of figure 1. Shear failure starts with the development of flexural cracks at the tension side of the beam. The load on the beam causes tension to increase on the tension side of the beam, damaging it and eventually causing cracks to form. Beams with adequate longitudinal reinforcement will fail in shear rather than flexure.

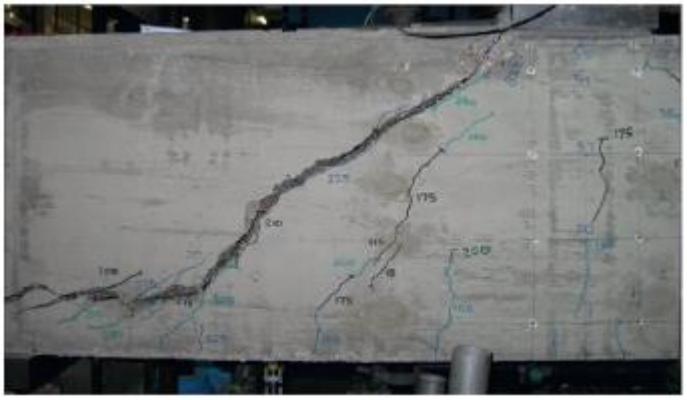

*Figure 1 (Vollum & Fang, 2014)*

As the loading increases, internal stresses in the beam start to rise, causing the flexural cracks to develop further. Eventually, the stresses are so high that the flexural cracks develop into shear cracks. Shear cracks are a result of planes being displaced relative to each other inside the beam. The flexural cracks are vertical at the bottom of the beam, but as they propagate, they turn towards the horizontal as shearing occurs diagonally. The shear crack develops until it reaches what is known as the critical point (Jeong et al. 2014).

At the critical point, the mechanisms that resist the shearing is the shear strength of the remaining un-cracked concrete chord, the remaining shear capacity of the crack and from any reinforcement that is present, which can come from either the shear capacity of the transverse reinforcement or from the dowel action of the longitudinal reinforcement.

Subsequently after dowel action, the concrete cover is subject to shearing. Due to the low shear capacity of unreinforced concrete, the cover cracks quickly, leading to spalling. At this point, the beam is close to failure.

If the load increases or is given time to deform the beam further, the last step before failure is the widening of the shear crack. This widening reduces the shear capacity of the crack, increasing the stresses on the other mechanisms that are resisting the shear, especially the un-cracked concrete chord. When the stress eventually becomes too high, the un-cracked concrete chord fails in shear and the beam has failed completely.

A point in a loaded beam is subject to beam action and arch action. Beam action is the moment acting on an area as a result of the changing stresses as one goes along the vertical axis of a beam. As a result of beam action, cracks at the extreme tension side of the beam are vertical.

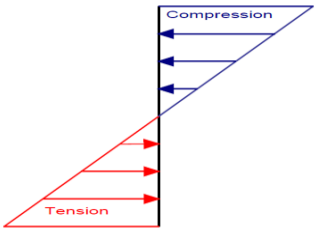


*Figure 2*

Consider the two fibres at either end of extreme tension and compression side, see figure 3. At the extreme tension side, the fibre is going to crack vertically (Figure 3a), while at the extreme compression side, it is going to split horizontally (Figure 3b). The crack first forms vertically, in flexure and as it propagates up the beam its starts to tilt towards to horizontal.

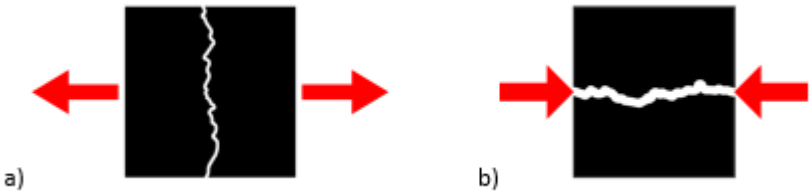


*Figure 3*

Arch action is due to difference in height of 2 section faces in combination with the sum of forces remaining constant through the section, see figure 4. This is why the shear taken by the un-cracked concrete chord increases as the crack propagates.

*Figure 4*

When arching action and beam action both affects a beam, the resultant force acting on the sections along the failure plane can be seen in figure 5. The shear capacity of the failure plane depends on the biaxial state of stresses it is subject to.

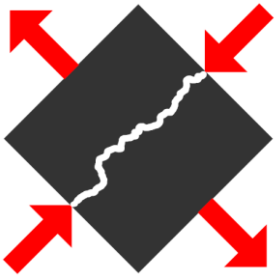

*Figure 5*

## 2.3 Kupfer's failure envelope

When an element is under stress from 2 directions, the element is considered to be under biaxial stress. When concrete is subject to this, the tensile and compressive strength of the concrete changes compared to when it is only under uniaxial stress.

Kupfer et al. (1969) investigated this phenomena by placing 20 cm*20 cm*5 cm concrete specimen under biaxial stresses (compression-compression, compression-tension and tension-tension). The concrete specimen had three different strengths, and stresses and strains were measured as the loads were increased.

It was discovered that stresses in one principal direction affected the strength of the concrete in the other different direction, see figure 6. This failure envelope is independent on the strength of the concrete, and regardless of strength, any concrete under compressive forces perpendicular to the principal plane, will be able to withstand higher stresses. This is known as Kupfer's failure envelope, a detailed view can be seen in figure 7.

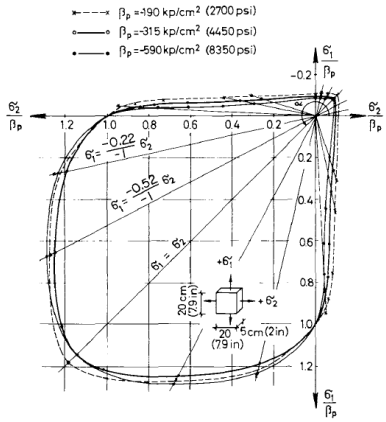


*Figure 6 Kupfer et al. (1969)*

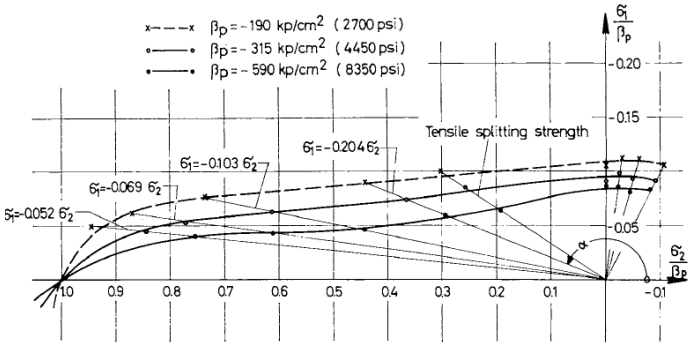


*Figure 7 Kupfer et al. (1969)*

Loads acting on beams distribute the weight of the load at a 45 degree fan from the application area. If one load is close enough to an adjacent load, the shear capacity of the beam they are acting on will increase. This is because the vertical internal stresses induced by the load pushes Kupfer's failure envelope further into the vertical compression area, increasing the concrete's capacity for resisting compressive stresses.

## 2.4 Kani's Valley

For a long time, it has been known that the shear capacity of beams is greatly increased when they are supporting loads near to their supports. In an effort to evaluate the effect of concrete strength, shear arm to depth ratio and reinforcement ratio on the shear capacity of reinforced concrete beams, Kani et al. (1966) discovered what is today known as Kani's valley.

His results showed that the strength of the beam increased as the shear arm ratio was reduced. See figure 8.

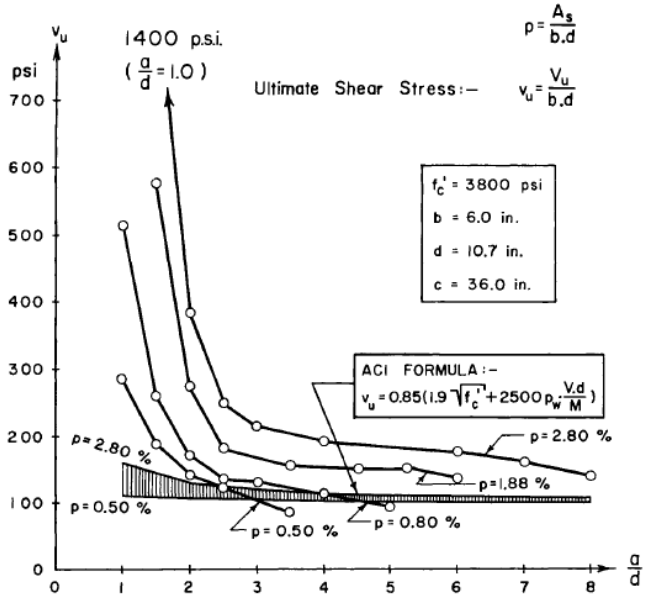


*Figure 8 Kani et al. (1966)*

Kani et al. (1966) observed that as the shear arm ratio approached 2.5, the beams started to fail in shear rather than flexure. Relative strength, $M_u/M_{fl}$, where $M_u$ is the maximum bending moment at failure, while $M_{fl}$ is the flexural strength of the beam was then plotted.

The experimental results showed that the relative strength is at its weakest when a/d is approximately 2.5, at approximately 50% strength, se figure 9 and 10. The relative strength would return to 100% at approximately a/d = 1 or 6.5, depending on concrete grade. When relative strength exceeds 100%, the flexural reinforcement will be fully utilised and the beam will fail in flexure rather than shear. The relative strength will then be assumed to be 100% and not the greater value.

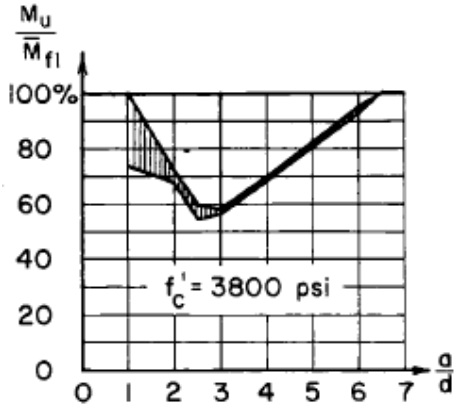


*Figure 9 Kani et al. (1966)*

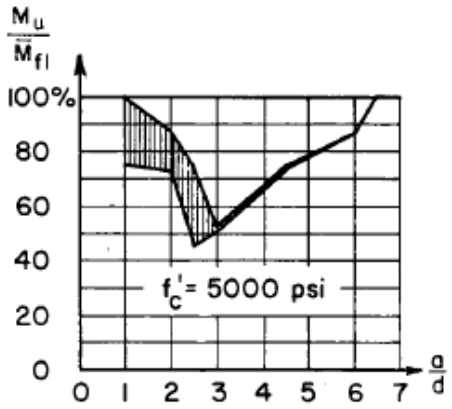


*Figure 10 Kani et al. (1966)*

Kani et al. (1966) concluded that the concrete strength had very little effect on the relative strength of the beam and that as one provided more reinforcement, the valley increased rapidly up until a 1.88% reinforcement ratio, see figure 11.

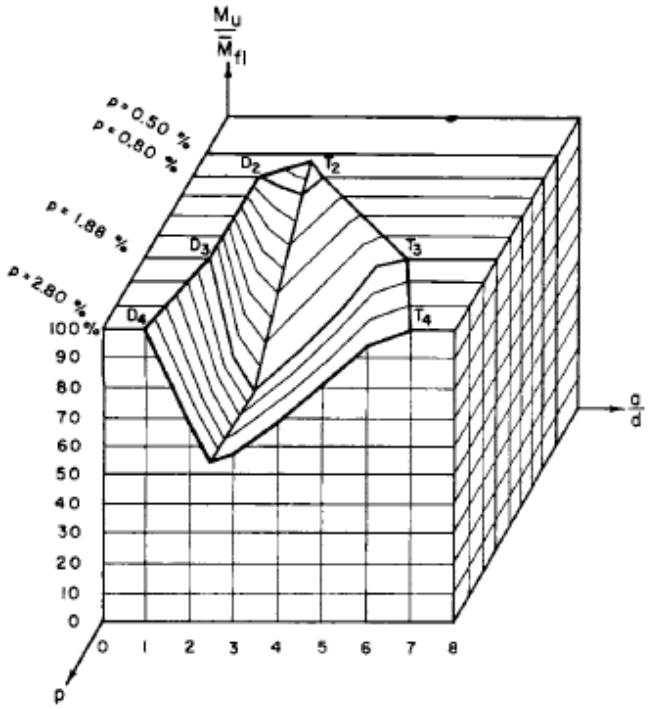


*Figure 11 Kani et al. (1966)*

## 2.5 Shear capacity of beams in EC-2

In EC-2, the shear capacity of a beam, $V_{Ed}$, comes either from the shear reinforcement or from the shear capacity of the concrete section. $V_{Ed}$ = Max ($\Sigma A_{sw} f_{yd}$, $V_{Rdc}$), where $\Sigma A_{sw} f_{yd}$ is the shear capacity of the reinforcement within the 3 central quarters of the shear span. $V_{Rd,c}$ is the shear capacity of the concrete without any reinforcement.

### 2.5.1 Shear resistance of beams without shear reinforcement

In Eurocode 2, the design shear capacity of a beam without shear reinforcement is governed by the shear capacity of the concrete $V_{Rd,c}$:

$$V_{Rd,c} = (C_{Rd,c}k(100 * \rho_l f_{ck})^{\frac{1}{3}} + k_1\sigma_{cp})b_w d \quad \text{Eq.2.1}$$

Where:

$$C_{Rd.c} = \frac{0.18}{\gamma_c} \quad \text{Eq.2.2}$$

$$k = (1 + \sqrt{\frac{200}{d}}) \leq 2.0, d \; in \; mm \quad \text{Eq.2.3}$$

$$\rho_l = \frac{A_{sl}}{b_w d} \leq 0.02 \quad \text{Eq.2.4}$$

$$k_1 = 0.15 \quad \text{Eq.2.5}$$

$$\sigma_{cp} = \frac{N_{Ed}}{A_c} < 0.2 \, f_{cd} \; (MPa) \quad \text{Eq.2.6}$$

$$V_{Rd,c} \geq (V_{min+}k_1\sigma_{cp})b_w d \quad \text{Eq.2.7}$$

$$v_{min} = 0.035k^{3/2}f_{ck}^{1/2} \quad \text{Eq.2.8}$$

Where $f_{ck}$ is the characteristic strength of concrete in MPa, k is a size factor, $\rho_l$ is the longitudinal reinforcement ratio, $b_w$ is the narrowest part of the cross-section in the tensile area in mm, $\sigma_{cp}$ is the concrete stress due to axial force, $N_{ed}$ is the axial force in the cross-section due to loading or prestressing [in N], $A_c$ is the area of concrete cross section [mm$^2$] and $V_{Rd,c}$ is in N. Values for $C_{Rd,c}$, $v_{min}$ and $k_1$ can be found in national annexes, the values listed above are the recommended values.

All the beams that will be investigated in this paper have constant cross sections and are not subject to any axial loads. Therefore, $b_w$ = b, and $N_{Ed}$ = 0, thus making $\sigma_{cp}$=0. Therefore, the shear resistance of unreinforced concrete beams can be simplified into:

$$V_{Rd,c} = \frac{0.18}{\gamma_c}(100 * \rho_1 f_{ck})^{\frac{1}{3}}(1 + \sqrt{\frac{200}{d}})bd \quad \text{Eq.2.9}$$

### 2.5.2 Shear resistance of beams with shear reinforcement

For members that require shear reinforcement, the shear capacity of the beam, $V_{Rd,s}$, is:

$$V_{Rd,s} = \min(\frac{A_{sw}}{s} * z * f_{ywd} * cot\theta \, , \frac{\alpha_{cw} * b_w * z * f_{cd} * v_1}{cot\theta + tan\theta}) \quad \text{Eq.2.10}$$

Where $A_{sw}$ is the cross-sectional area of the shear reinforcement, s is the stirrup spacing, $f_{ywd}$ is design yield strength of the shear reinforcement, $v_1$ is a strength reduction factor for concrete

cracked in shear and $\alpha_{cw}$ is a coefficient that takes into account the state of stress in the compression chord. $\alpha_{cw}$ is 1 for non-pre-stressed beams. Because all safety factors are removed, $f_{cd} = f_{yd}$.

$$v_1 = 0.6 * (1 - \frac{f_{ck}}{250}) \quad \text{Eq.2.11}$$

### 2.5.3 Loads near supports

When a load is applied on the upper side of the beam at a distance $a_v$ and $0.5d \leq a_v \leq 2d$, the shear force $V_{Ed}$ is reduced by $\beta = a_v/2d$. This is only valid when the reinforcement is fully anchored at the support. A shear force calculated this way must satisfy the following condition:

$$V_{Ed} \leq A_{sw} * f_{ywd} * sin\alpha \quad \text{Eq.2.12}$$

Where $A_{sw}*f_{ywd}$ is the central three quarters of the shear arm $a_v$, when $a_v > 0.5$, $a_v = 0.5$.

# Chapter 3. Proposed model

## 3.1 Model introduction

The new model, proposed by Mari et al. is a semi-empirical mechanically based model. It attempts to predict shear-flexure failure of reinforced concrete beams with and without stirrups. The model assumes that the beam subject to an incremental load fails in the same manner as described in section 2.2, *Shear transfer mechanisms*. The shear crack will fail as described there, but it is assumed that a second crack develops inside the concrete chord above the neutral axis, which subsequently propagates down to the critical shear crack, causing failure.

For beams without shear reinforcement, the model is based on a strut and tie model. The concrete ties and struts preserve the static equilibrium. It is assumed that the concrete ties have some tensile capacity after cracking, provided that the crack is sufficiently narrow. This tensile capacity comes from shear transferred along the crack and residual tensile capacity. As cracks propagate throughout the beam, the concrete ties change in inclination to avoid the widest cracks, thus preserving the static equilibrium.

Increasing the load causes crack widths to increase, thus concentrating tensile stresses further up in the beam where the crack width is smaller. The effect of this is that the angle of the ties with respect to the horizontal, α, increases. This increasing in angle reduces the amount of shear resisted along the crack, $V_w$ and the increment of force resisted at the longitudinal reinforcement, ΔT. In order to preserve static equilibrium, when ΔT lessens, so does ΔC, where c is the compression force in the un-cracked concrete chord. This causes the inclination of the strut (strut BD in figure 12a and b) to increase in order to compensate for the loss of shear resisted over the crack. This in turn causes arching acting in the un-cracked concrete chord, thus increasing the shear taken by the concrete chord.

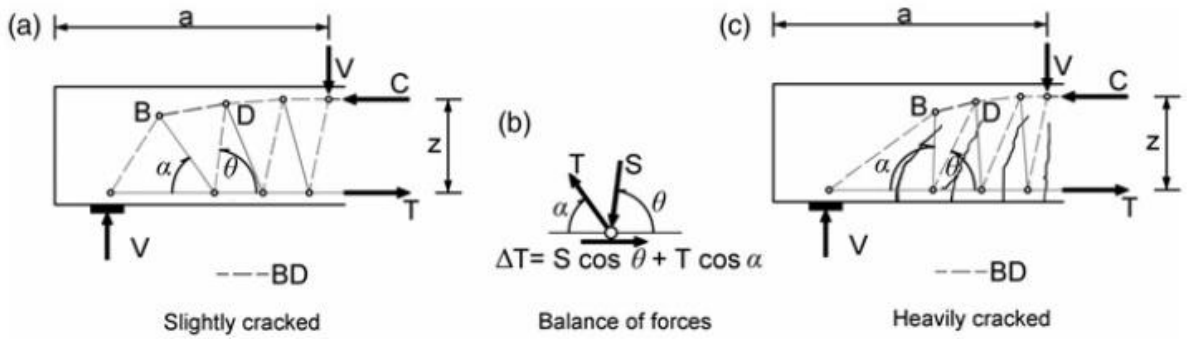


*Figure 12 Mari et al. (2014)*

If reinforcement is present, the stirrups take on the role previously held by the concrete tie. In addition, stirrups restrain the widening of cracks by friction and residual stresses, they vertically confine the concrete, increasing its shear strength and connecting the longitudinal reinforcement, increasing its shear capacity.

The beam action in the beam is caused by the difference in stresses on either side of a region, see figure 13 b. The arching action is caused by a difference in the height of the regions faces, $x_1$ and $x_2$ which causes stresses to redistribute, thus creating stresses on the region.

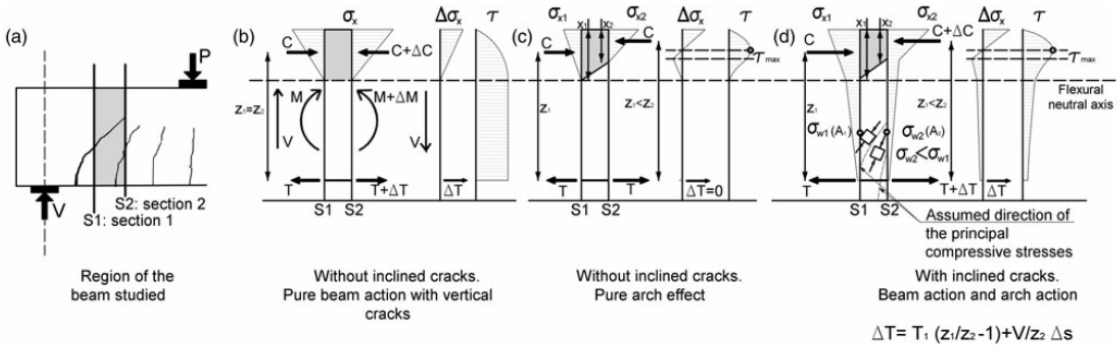


*Figure 13 Mari et al. (2014)*

## 3.2 Model assumptions and their validity

1) During ultimate load levels, the shear and bending is resisted by the un-cracked concrete chord ($V_C$), the longitudinal ($V_l$) and transverse ($V_s$) reinforcement and the aggregate interlocking action ($V_w$) along the crack.

2) The distribution of stresses along the concrete chord have been assumed to be as depicted in figure 14. The horizontal stresses are linearly distributed, with the maximum normal stress at the extreme compressive fibre, located at the top of the beam.

   The vertical stresses are assumed to be bilinear, 0 at the top fibre and maximum in the middle of the un-cracked concrete chord, at 0.5 x. After this it is assumed to be constant.

   The shear stress distribution is assumed to be parabolic and 0 at the top fibre and at the neutral axis. Maximum shear is assumed to be at y = x/2. Theoretically, the shear is 0 at the bottom fibre at the beam and more than 0 at the neutral axis. However, the simplified shear distribution is similar to the theoretical distribution and therefore used.

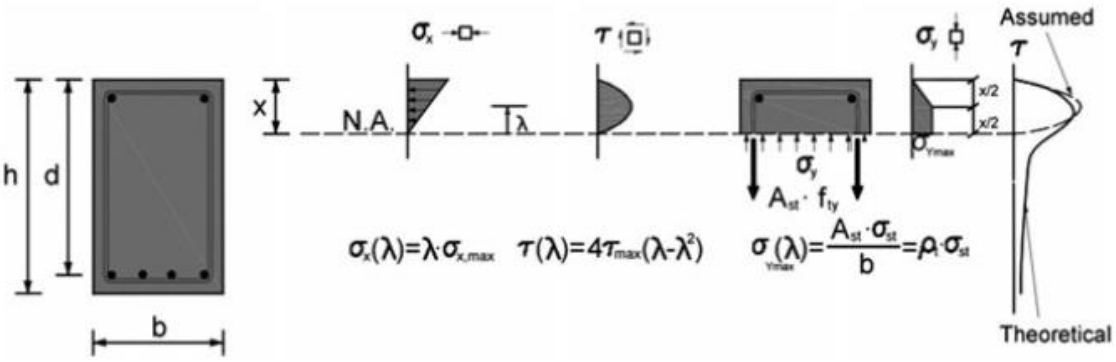


*Figure 14 Mari et al. (2014)*

3) The depth of the un-cracked zone is equal to the neutral axis in bending.

4) The beam is subject to biaxial stresses, and anytime the un-cracked concrete experiences stresses that exceed Kupfer's failure envelope, it fails.

5) The horizontal projection of the shear crack is considered to be 0.85d, see figure 15.

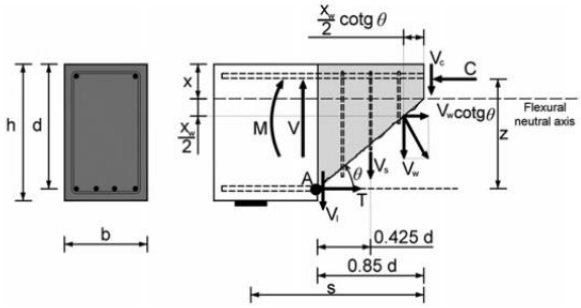


*Figure 15 Mari et al. (2014)*

6) At the ultimate limit state, all existing stirrups have yielded.

7) All longitudinal reinforcement is considered to be anchored, making all reinforcement effective at the critical shear section.

## 3.3 Location of the critical point

The point in the concrete chord where failure will initiate is known as the critical point. Failure will initiate at the point of maximum damage as defined by equation 3.17. Studies (Mari et al.,2014, Swamy & Quereshi, 1974) have shown that this can be found at approximately y = 0.425x from the neutral axis if linear or parabolic stress distributions are assumed. This is valid for s/d = M/((V*d) < 3.0. Values for the relative distance to the neutral axis, y/x have been plotted in figure 16 below, where relative damage is the ratio between the damage of a fibre at a distance from the neutral axis and the damage at the top compressed fibre.

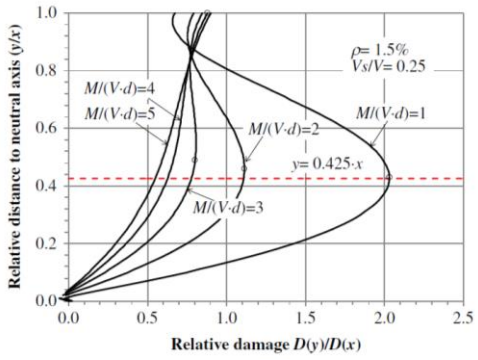


*Figure 16 Mari et al. (2014)*

The weakest section of a beam subject to shear-bending failure is found at the tip of the first diagonal shear crack, at C, see figure 17. It forms at this location as any point closer to 0 bending moment will have more of the un-cracked concrete chord to resist shear, while any point closer to the load will experience higher normal stresses which increases the shear transfer capacity of the point.

The initiation of the flexural cracking is assumed to start when $S_{cr}= M_{cr}/V_u$, where $S_{cr}$ is distance from the support that the flexural crack initiates, $M_{cr}$ is the cracking moment and $V_u$ is the ultimate shear load. According to the 5$^{th}$ assumption of the model, the crack propagates 0.85d, where the critical section is found. This position for the critical section was found by Park et al. (2006).

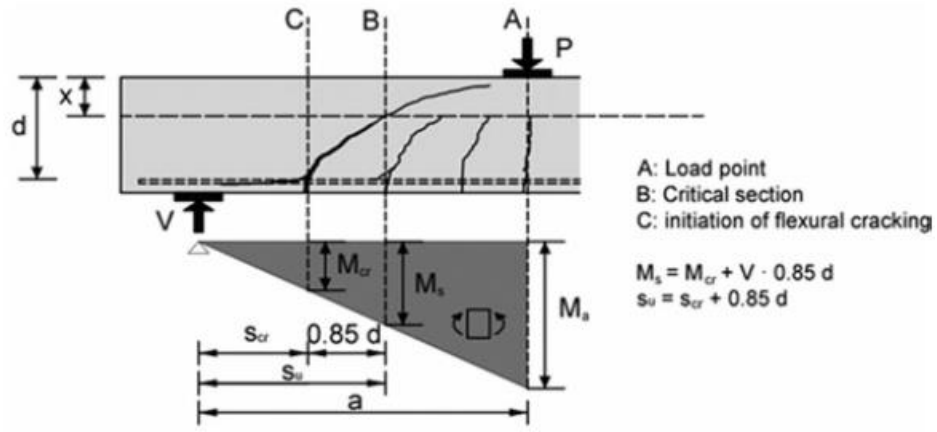


*Figure 17 Mari et al. (2014)*

## 3.4 Shear-flexural strength of beams subject to point loads

The shear strength of the beam is calculated at the critical section. Here, the equilibrium between the internal forces (V, M), the stresses at the un-cracked concrete chord ($V_c$, C), along the crack ($V_w$), the stirrups ($V_s$), and the longitudinal reinforcement ($V_l$, T) is taken about point A. See figure 15.

$$C = T + V_w * tan\theta \quad \text{Eq. 3.1}$$

$$V = V_c + V_w + V_l + V_s \quad \text{Eq. 3.2}$$

$$M = C * z = M + V_c * 0.85 * d + \frac{V_w*(0.85*d-0.5*x_w*cot\theta)}{cos^2\theta} + 0.5V_s * 0.85 * d \quad \text{Eq. 3.3}$$

The non-dimensional shear carried by the un-cracked concrete chord, $v_c$, can be found by substituting equation 3.38, 3.40 and 3.41 into equation 3.14, this gives:

$$v_c = \frac{V_c}{f_{ct}*b*d} = R_t * k_\lambda * \xi * \sqrt{1 - \frac{\lambda*(0.4+1.7*v_c+2*v_w*\frac{0.85-\xi_w*cot\theta}{cot^2\theta}+v_s*0.85}{\xi*\left(1-\frac{\xi}{3}\right)*R_t}\left(\frac{v_s}{0.85*R_t}-1\right) - \frac{v_s}{0.85*R_t}} \quad \text{Eq. 3.4}$$

Here, $R_t$ is the ratio between principal tensile stress, $\sigma_1$, and the tensile strength of the concrete at failure. According the equation 3.17 this equals:

$$R_t = \frac{\sigma_1}{f_{ct}} = (1 - 0.8 * \frac{\sigma_2}{f_{cc}}) \quad \text{Eq. 3.5}$$

$R_t$ depends on the principal stress, which depends on the shear force, $V_c$, so equation 3.4 must be solved iteratively by assuming $R_t$=1 and the solving and resolving equation 3.4 until convergence. Figure 18 shows the solution for different values of $v_s$ and neutral axis depth. The solutions follow a clearly linear trend, but a size factor must be introduced to take into account due to the brittle nature of the failure. The linear relationship between neutral axis depth and dimensionless shear force to predict the amount of shear transferred through the concrete reinforcement was previously been observed in other studies (Tureyen & Frosch, 2003, Zararis & Papadakis, 2001).

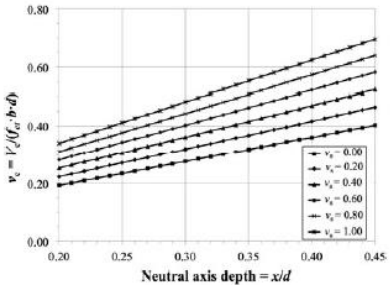


*Figure 18 Mari et al. (2014)*

The size factor, ζ, is the one used Zararis & Papadakis and depends on the shear span, a:

$$\zeta = 1.2 - 0.2 * a = 1.2 - 0.2 * \frac{a}{d} * d \geq 0.65 \qquad \text{Eq. 3.6}$$

Adding this size effect to the dimensionless shear force, the linear relationship of the dimensionless shear force to neutral axis depth can be approximated into:

$$v_c = \zeta((0.88 + 0.70 * v_s) * \frac{x}{d} + 0.02) \qquad \text{Eq. 3.7}$$

## 3.5 Fracture Energy

Fracture energy, $G_f$. is an important parameter for the proposed model. It is used to determine the shear capacity of the shear reinforcement. The Model Code (Fédération Internationale du Béton, 2013) states that fracture energy can be expressed as a function of mean concrete compressive strength, while Wittman (2002) proposed that it can be expressed as a function of maximum aggregate size. Mari et al. (2014) decided to draw from both and derived a new expression for the fracture energy, which results are identical to that of the Model Code 2010 for $d_{max}$ = 20 mm and close to Wittman's results.

$$G_f = 0.028 * f_{cm}^{0.18} * d_{max}^{0.32} \qquad \text{Eq. 3.8}$$

It should be noted that Sagaseta et al. (2010) did not find that difference in aggragte types affect the strength or crack patterns of beams. It was concluded that the orientation and position of the shear crack, which is random had a large effect on shear strength.

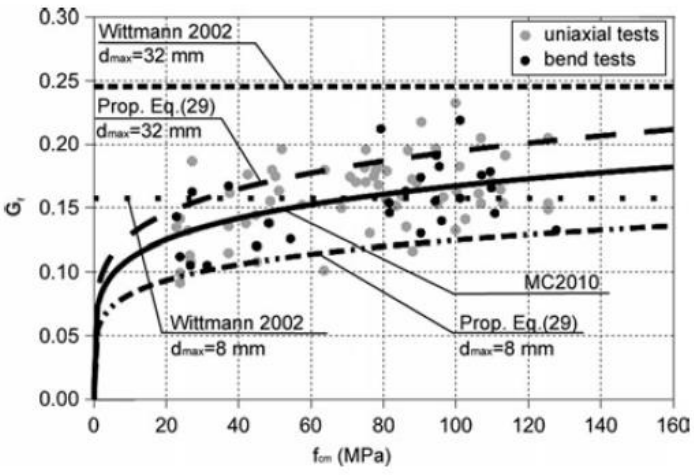


*Figure 19 fib Task Group 8.2 (2008)*

## 3.6 Shear transfer mechanisms

### 3.6.1 Shear capacity of the un-cracked concrete chord, $V_c$

The principal tensile and compressive stresses produced by normal stress ($\sigma_x$ and $\sigma_y$) and shear stress ($\tau$) at any point is according to Mohr's circle defined as:

$$\sigma_{1,2} = \frac{\sigma_x+\sigma_y}{2} \pm \sqrt{(\frac{\sigma_x-\sigma_y}{2})^2 + \tau^2} \quad \text{Eq. 3.9}$$

$$\tau = \sigma_1 \sqrt{1 - \frac{\sigma_x+\sigma_y}{\sigma_1} + \frac{\sigma_x*\sigma_y}{\sigma_1^2}} \quad \text{Eq. 3.10}$$

If a point, at a known distance λ*x, from the neutral axis of the concrete chord where, x is the distance from the neutral axis and the shear stress $\tau_\lambda$ is known, the shear stress distribution ($\tau(y)$) along the un-cracked concrete can be obtained. They can be found by imposing the following boundary conditions, $\tau(0)=0$, $\tau(x)=0$ and $\tau(\lambda*x)= \tau_\lambda$. This gives:

$$\tau(y) = \frac{\tau_\lambda}{\lambda*(1-\lambda)} (\frac{y}{x} - \frac{y^2}{x^2}) \quad \text{Eq. 3.11}$$

The shear force along the concrete chord $V_c$ is obtained by assuming a constant width along the chord and integrating the shear stress along the un-cracked concrete chord.

$$V_c = \int_0^x \tau(y) * b * dy = \frac{\tau_\lambda * b * x}{6*\lambda*(1-\lambda)} \quad \text{Eq. 3.12}$$

Substituting τ (y) from equation 3.11 yields the final expression for the shear strength of the un-cracked concrete chord.

$$V_c = \int_0^x \frac{\tau_\lambda}{\lambda*(1-\lambda)} (\frac{y}{x} - \frac{y^2}{x^2}) * b * dy = \frac{\tau_\lambda * b * x}{6*\lambda*(1-\lambda)} \quad \text{Eq. 3.13}$$

$$V_c = K_\lambda * b * x * \tau = \sigma_1 \sqrt{1 - \frac{\sigma_x+\sigma_y}{\sigma_1} + \frac{\sigma_x*\sigma_y}{\sigma_1^2}} \quad \text{Eq. 3.14}$$

Where:

$$K_\lambda = \frac{1}{6*\lambda*(1-\lambda)} \quad \text{Eq. 3.15}$$

The neutral axis depth can be obtained through standard analysis of cracked reinforced concrete sections under flexure only. If the section does not have any compressive reinforcement, the neutral axis depth is given by:

$$\xi = \frac{x}{d} = \alpha_e * \rho * (-1 + \sqrt{1 + \frac{2}{\alpha_e * \rho}}) \quad \text{Eq. 3.16}$$

$\alpha_e = E_s/E_c$, which is the modular ratio between steel and concrete. $P = A_s/(b*d)$, which is the longitudinal reinforcement ratio.

Failure occurs when the principal stresses reach Kupfer's failure envelope in the compression-tension branch. In the branch, the failure envelope is considered to be straight until the uniaxial compressive concrete strength, $f_{cc}$ reaches 0.8, or 80% of max compressive capacity.

$$\frac{\sigma_1}{f_{ct}} + 0.8 * \frac{\sigma_2}{f_{cc}} = 1 \qquad \text{Eq. 3.17}$$

### 3.6.2 Shear capacity of the crack, $V_w$

Shear transferred across the crack is done so either through residual tensile stresses acting across the crack or through frictional stresses acting along the crack as the rough crack surfaces slide against each other. Both factors are caused by the irregularities in the crack. The residual tensile stress is the crack's capacity to hold tensile forces. This capacity falls as the crack width increases and is generally considered to be small.

When vertical loads are applied near the shear crack, the crack faces get pushed together, thus constricting sliding. Sliding between to internal planes is the cause of shear, so vertical loads increase the shear capacity of the concrete. Tests done by Vollum & Fang (2014) confirmed this, and their results can be seen in figure 20. This increase in concrete shear strength is not included in the general model, but is applied for spesial cases where beams are subject to multiple point loads, see section 3.8.

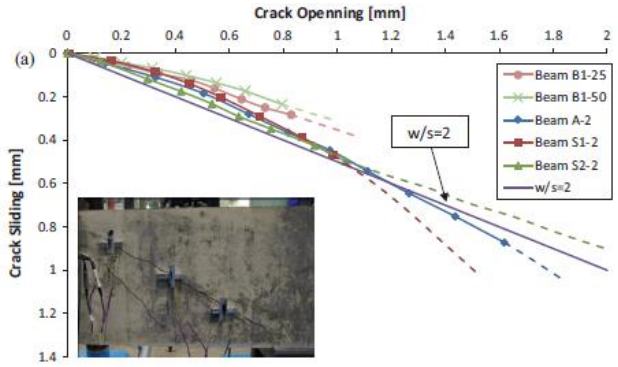


*Figure 20 Vollum & Fang (2014)*

In order to evaluate the stresses transferred across the crack, the following procedure was adopted by Mari et al. (2014).

1) Compatibility of strains normal to the crack is assumed.

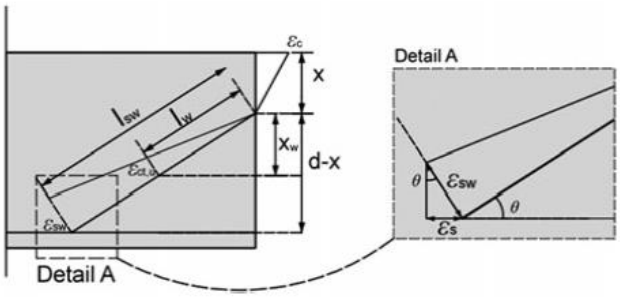


*Figure 21 Mari et al. (2014)*

2) The tensile stress-strain relationship is assumed to peak at $\varepsilon_{ct,cr}$, when the stress reaches $f_{ct}$, before linearly falling to 0, at $\varepsilon_{ct,u}$. $\varepsilon_{ct,u}$ depends on the fracture energy of the concrete.

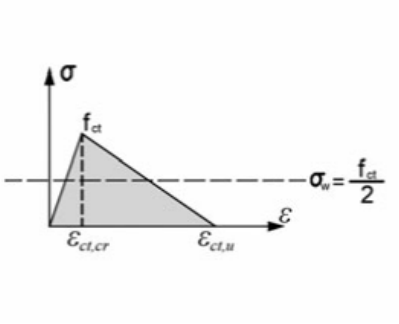


*Figure 22 Mari et al. (2014)*

3) It is assumed that the larger the crack width, the lower the residual tensile stress. This relationship was considered to be linear, allowing the fracture energy to be found more easily.

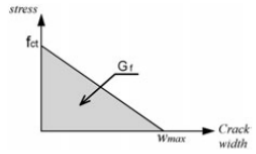


*Figure 23 Mari et al. (2014)*

4) The crack opening width is obtained by multiplying the tensile strain of concrete ($f_{ct}$) by the mean length between inclined cracks ($s_{m\theta}$). The mean length between inclined cracks vary at different locations of the cracks and is affected by the presense of transverse and longitudinal reinforcement. Not all the flexural cracks develop into shear cracks, the distance between shear cracks is greater. It is therefore assumed that the average crack spacing is equal to the effective depth of the element.

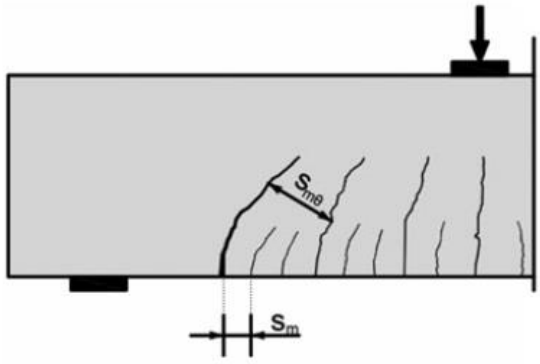


*Figure 24 Mari et al. (2014)*

The shear force ($V_w$) resisted along the crack is the integral of the normal stresses, $\sigma_w$, the crack width, b and the crack angle, θ, across the length of the crack, $l_w$, where the tensile stresses are active.

$$V_c = \int_0^{l_w} \sigma_w * b * cos\theta * dl \approx \frac{x_w}{sin\theta} * \sigma_w * b * cos\theta = x_w * \sigma_w * b * cot\theta \qquad \text{Eq. 3.18}$$

$\sigma_w$ is defined as the normal stress in a horizontal fibre in the cracked web. $\sigma_w = f_{ct}/2$ along the length of the crack with residual stress. This makes it energetically equivalent to the triangular stress distribution obtained with assumption 3.

The length the tensile zone is obtained by using the crack strain and geometrical relationships, see figure 25.

$$x_w = (d - x) * \frac{\varepsilon_{ct,u}}{\varepsilon_s} * sin^2\theta \qquad \text{Eq. 3.19}$$

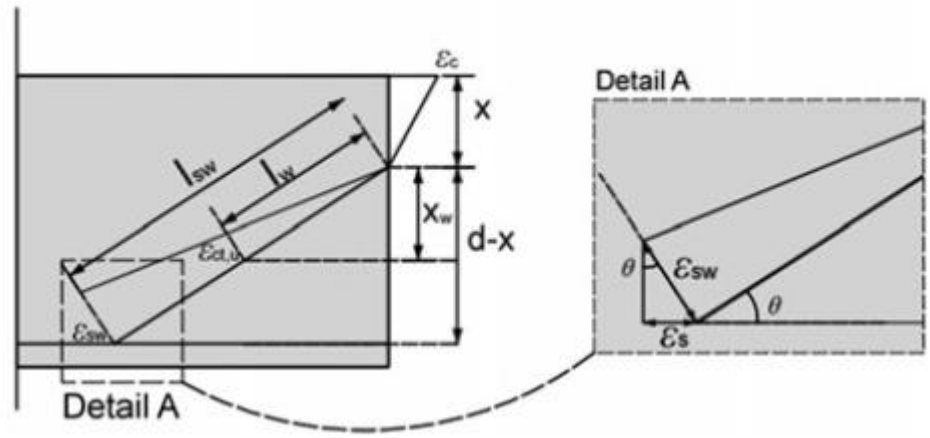


*Figure 25 Mari et al. (2014)*

By substituting equation 3.19 into equation 3.20 and taking equation 3.25 into account, the shear force becomes:

$$V_w = 0.425 * f_{ct} * b * d * \frac{\varepsilon_{ct,u}}{\varepsilon_s} * sin^2\theta \qquad \text{Eq. 3.20}$$

The fracture energy of the concrete is the area of the triangle found in figure 23.

$$G_f = \int_0^w \sigma(w) * dw \approx 0.5 * f_{ct} * w_{max} = 0.5 * f_{ct} * \left(\varepsilon_{ct,u} - \varepsilon_{ct,cr}\right) * s_{m\theta} \qquad \text{Eq. 3.21}$$

The largest crack opening, $w_{max}$ is assumed to be:

$$w_{max} = 0.5 * f_{ct} * \left(\varepsilon_{ct,u} - \varepsilon_{ct,cr}\right) * s_{m\theta} \qquad \text{Eq. 3.22}$$

Equation 3.21 can then be expressed as:

$$\varepsilon_{ct,u} = \varepsilon_{ct,cr} + \frac{2*G_f}{f_{ct}*s_{m\theta}} = \frac{f_{ct}}{E_c} + \frac{2*G_f}{f_{ct}*s_{m\theta}} = \frac{f_{ct}}{E_c} * (1 + \frac{2*G_f*E_c}{f_{ct}^2*s_{m\theta}}) \qquad \text{Eq. 3.23}$$

Finally, the shear transferred along the crack can be expressed in non-dimensional terms as:

$$v_w = \frac{V_W}{f_{ct}*b*d} = \frac{0.425*sin^2\theta*f_{ct}}{E_C*\varepsilon_s}(1 + \frac{2*G_f*E_c}{f_{ct}^2*s_{m\theta}}) \qquad \text{Eq. 3.24}$$

$$cot\theta = \frac{0.85*d}{(d-x)} = \frac{0.85}{(1-\xi)}$$ Eq. 3.25

Where:

$$\xi = \frac{x}{d}$$ Eq. 3.26

$$v_w = \frac{V_w}{f_{ct}*b*d} = 167 * \frac{f_{ct}}{E_c} * (1 + \frac{2*E_c*G_f}{f_{ct}^2*d})$$ Eq. 3.27

### 3.6.3 Shear capacity of the longitudinal reinforcement, $V_l$

When an element is loaded, the longitudinal reinforcement is subject to a vertical displacement, causing crack sliding and propagation. The longitudinal reinforcement has a small (Kotsovos et al., 1987; Zararis & Papdakis,2001) shear capacity by its own, but if stirrups are present this capacity is greatly increased. This is due to the vertical constraint the stirrups provide on the longitudinal reinforcement.

Consider the relative vertical displacement between the 2 edges of a crack opening. This displacement is the sum of the crack opening ($\delta_m$) and the crack sliding ($\delta_v$).

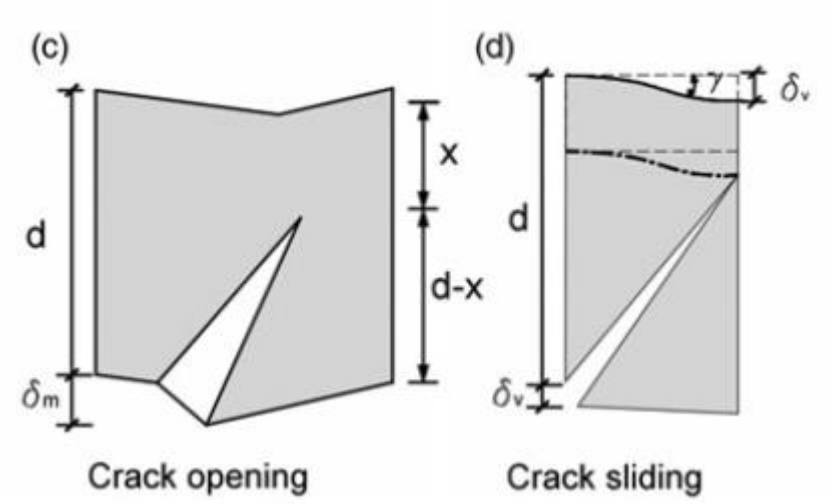


*Figure 26 Mari et al. (2014)*

Then the crack opening can be expressed as:

$$\delta_m = w_x * cot\theta = \varepsilon_{sx} * s_{mx} * cot\theta \approx 0.72 * d * \frac{\varepsilon_{sx}}{1-\xi}$$ Eq. 3.28

Crack sliding is due to the distortion of the un-cracked concrete part of the element and the vertical displacement due to this is:

$$\delta_v = \gamma * 0.85 * d$$ Eq. 3.29

Combining these 2 expressions and considering the ratio between the shear stress and the axial tensile strain to be $\gamma/\varepsilon_{sx}$, the following expression is obtained:

$$\frac{\gamma}{\varepsilon_{sx}} = \frac{\frac{6*V_c}{5*b*x*G_c}}{\frac{M}{E_S*A_S*(d-\frac{x}{3})}} \approx 2.64 * \frac{V_c*d}{M} * \frac{\alpha_e*\rho*(1-\frac{\xi}{3})}{1-\xi} \quad \text{Eq. 3.30}$$

Equation 3.28, 3.29 and 3.30 can then be rearranged to:

$$\delta = \delta_m + \delta_v = 0.72 * d * \frac{\varepsilon_{sx}}{1-\xi}(1 + 3.1 * \frac{V_c}{M} * \alpha_e * \rho * \left(1 - \frac{\xi}{3}\right)) \quad \text{Eq. 3.31}$$

Which can be simplified into:

$$\delta = 0.8 * d * \frac{\varepsilon_{sx}}{1-\xi} \quad \text{Eq. 3.32}$$

This imposed displacement produces a shear force, $V_l$ approximately equal to:

$$V_l = \frac{12*E_S*n_b*I_s*\delta}{s_t^3} = \frac{12*E_S*n_b*\pi*\phi^4*\delta}{s_t^3*64} \approx 0.64 * \frac{E_S}{f_{ct}} * \rho * \frac{\phi^2*d}{s_t^3} * \frac{\varepsilon_{sx}}{1-\xi} \quad \text{Eq. 3.33}$$

By assuming that $\phi/s_t = 0.15$, $d/s_t=2$, $\varepsilon_{sx} = 0.0009$ and $E_c/f_{ct} = 10000$, this expression can be simplified into a non-dimensional term:

$$v_l = \frac{V_l}{f_{ct}*b*d} \approx 0.23 * \frac{\alpha_\varepsilon*\rho}{1-\xi} \approx 0.25 * \xi - 0.05 \quad \text{Eq. 3.34}$$

### 3.6.4 Shear capacity of the transverse reinforcement, $V_s$

In the proposed model, it is assumed that any stirrups present have yielded at failure, thus

$$V_s = 0.85 * d * A_{sw*} f_{yw} \quad \text{Eq. 3.35}$$

This can be expressed in non-dimensional terms as $v_s$.

$$v_s = \frac{V_s}{f_{ct}*b*d} = \frac{0.85*d*A_{sw*}f_{yw}}{f_{ct}*b*d} = 0.85 * \rho_w * \frac{f_{yw}}{f_{ct}} \quad \text{Eq. 3.36}$$

### 3.6.5 Stresses at the critical point

By using classical flexural analysis, the normal stresses ($\sigma_x$) in the concrete compression chord can be expressed as:

$$\sigma_x = \frac{2*\lambda*M}{b*x*(d-\frac{x}{3})} = \frac{2*\lambda*(M+V_c*0.85*d+\frac{V_w*(0.85*d-0.5*x_w*cot\theta)}{cos^2\theta}+0.425*V_s*d}{b*x*(d-\frac{x}{3})} \quad \text{Eq. 3.37}$$

Dividing by $f_{ct}*b*d^2$, a non-dimensional expression is found:

$$\frac{\sigma_x}{f_{ct}} = \frac{\lambda*(2*\mu+1.7*v_c+2*v_w*\frac{0.85-\xi_w*cot\theta}{cot^2\theta}+v_s*0.85}{\xi*(1-\frac{\xi}{3})} \quad \text{Eq. 3.38}$$

The cracking moment to be considered is the cracking moment, $M_{cr}$, which in non-dimensional terms is expressed as:

$$\mu_{cr} = \frac{A_{sw}*f_{yw}}{f_{ct}*b*d^2} = \frac{b*h^2*f_{ct}}{6*f_{ct}*b*d^2} = \frac{1}{6} * (\frac{h}{d})^{2 \simeq 0.2} \quad \text{Eq. 3.39}$$

Consider the horizontal cut shown in figure 15, where the equilibrium is balanced by tensile forces in the stirrups and the vertical concrete stress ($\sigma_y$).

$$\frac{\sigma_y}{f_{ct}} = \frac{A_{sw} * f_{yw}}{f_{ct} * b} = \frac{V_s}{0.85 * f_{ct} * b * d} = \frac{v_s}{0.85} \quad \text{Eq. 3.40}$$

At the critical point of the un-cracked concrete chord, the shear stress, $\tau_\lambda$ is:

$$\tau_\lambda = \frac{6 * V_c}{b * x} * (\lambda - \lambda^2) = \frac{1.47 * V_c}{b * x} \quad \text{Eq. 3.41}$$

## 3.7 Total beam strength

In summation the beam gets its shear strength (V) from the following; the shear capacity of the un-cracked concrete chord ($V_c$), the shear force resisted along the crack, ($V_w$), the shear capacity of the longitudinal reinforcement ($V_l$) and the shear strength of the transverse reinforcement ($V_s$).

$$V = V_c + V_w + V_l + V_s = f_{ct} * b * d * (v_c + v_w + v_l + v_s) \quad \text{Eq. 3.42}$$

$v_c = \xi * ((0.88 + 0.70 v_s) * \frac{x}{d} + 0.02)$ Eq. 3.7

$v_w = \frac{V_w}{f_{ct} * b * d} = 167 * \frac{f_{ct}}{E_c} * (1 + \frac{2 * E_c * G_f}{f_{ct}^2 * d})$ Eq. 3.27

$v_l = \frac{V_l}{f_{ct} * b * d} \approx 0.23 * \frac{\alpha_e * \rho}{1 - \xi} \approx 0.25\xi - 0.05$ Eq. 3.34

$v_s = = \frac{V_s}{f_{ct} * b * d} = 0.85 \rho_w * \frac{f_{yw}}{f_{ct}}$ Eq. 3.36

By taking $v_s$ and $v_l$ as 0, the shear strength of beams and one way slabs without shear reinforcement is obtained: Taking into account all the factors contributing to the shear strength of the beam, $V_{u,0}$ is obtained:

$$V_{u,0} = f_{ct} * b * d * (v_c + v_w + v_l + v_s) \quad \text{Eq. 3.43}$$

## 3.8 Adaptation for beams close to supports

The general expression for shear force obtained in equation 3.42, is only valid for beams where a/d > 2.5, and there are no interaction between multiple loads. Mari et al. (2014) have made special provision for this case where the ultimate shear strength, $V_u$, of the beam with a load close to the support can be expressed as:

$$V_u = V_{cu} + V_{su} \quad \text{Eq. 3.44}$$

Where:

$$V_{cu} = \zeta \frac{x}{d} K_p \left[ 0.30 \frac{f_{ck}^{2/3}}{\gamma_c} + \frac{V_{su}}{b \cdot d} + \sigma_{cv} \right] bd \quad \text{Eq. 3.45}$$

$$V_{su} = \frac{A_{sw}}{s} f_{ywd} (d - x) \, sin\alpha \, (cot\theta + cot\alpha) \quad \text{Eq. 3.46}$$

Where $k_p$ =1, s is the stirrup spacing, $\sigma_{cv}$ is the increase in shear strength capacity of the concrete due to nearby loads, and is only valid when the distance between the loads is less than $0.5(s_0 + a_v/d \cdot x_1)$

$$\sigma_{cv} = \frac{0.85 * Q_d}{b(s_0 + \frac{a_v * x_1}{d})} = \frac{0.85 * Q_d}{b(s_0 + a_v * \frac{x_1}{d})} \quad \text{Eq. 3.47}$$

$$COT\theta = \frac{a_v}{d} < \frac{0.85*d}{d-x_1} \quad \text{Eq. 3.48}$$

$$\frac{x_1}{d} = \frac{x}{d} + \left(1 - \frac{x}{d}\right) * (1 - 0.4 * \frac{a_v}{d})^2 \quad \text{Eq. 3.49}$$

$$\frac{x}{d} = \alpha_e * \rho_l(-1 + \sqrt{1 + \frac{2}{\alpha_e * \rho_l}}) \quad \text{Eq. 3.50}$$

Where $Q_d$ is the load applied, θ is the angle between the vertical and the inclination of the direct strut, $x_1$ is the neutral axis in the d-region and $x_o$ is the neutral axis in the b-region. If multiple loads are applied on at each half of the beam, multiple shear failure planes exist, so the most critical shear plane must be determined and used as the failure plane.

## 3.9 Previous data and results

Mari et al. (2014) compared the accuracy of their proposal against the predictions of Eurocode 2, ACI318-08 and Model Code 2010, using the large data base, based on the publication of Collins et al (2008), Cladera & Mari (2007) and Yu & Bazant (2011). The first publication was used for concrete beams without stirrups while the latter were used for concrete beams with stirrups. A total of 892 beams without stirrups and 239 beams with stirrups were evaluated. All of the beams failed in shear and all the beams without shear reinforcement had an a/d-ratio greater or equal to 2.5. Any safety factors used in the models were removed (taken as 1) when the models were evaluated against each other and the data. The range of variables can be seen in table 1 below.

| | 892 beams without stirrups | | 239 beams with stirrups | |
|---|---|---|---|---|
| | Min | Max | Min | Max |
| $b$ (mm) | 21 | 3000 | 76 | 457 |
| $d$ (mm) | 41 | 2000 | 95 | 1890 |
| $f_c$ (MPa) | 6 | 127 | 13 | 125 |
| $\rho$ (%) | 0.1 | 6.6 | 0.5 | 7.0 |
| $\rho_w = A_{st} \cdot f_{yw}/b$ (MPa) | – | – | 0.1 | 8.1 |
| $a/d$ | 2.5 | 8.5 | 2.4 | 5.1 |
| $V_{test}$ (kN) | 2 | 1295 | 14 | 2239 |

*Table 1*

The results obtained by Mari et al can be seen in table 2 and 3. The proposed model generally had the lowest coefficients of variation. The predictions of the results were compared in a large database of experiments published by Collins et al. (2008).

| | 892 beams without stirrups | | | | 239 beams with stirrups | | | |
|---|---|---|---|---|---|---|---|---|
| $V_{test}/V_{pred}$ | EC-2 | ACI 318-08 | MC10 Lev II | Proposal | EC-2 | ACI 318-08 | MC10 Lev III | Proposal |
| Average | 1.07 | 1.28 | 1.20 | 1.04 | 1.72 | 1.25 | 1.21 | 1.02 |
| Median | 1.03 | 1.27 | 1.16 | 1.01 | 1.61 | 1.24 | 1.20 | 1.01 |
| Standard deviation | 0.226 | 0.346 | 0.223 | 0.179 | 0.638 | 0.262 | 0.225 | 0.169 |
| COV (%) | 21.12 | 27.11 | 18.61 | 17.28 | 37.13 | 21.04 | 18.58 | 16.60 |
| Minimum | 0.66 | 0.38 | 0.74 | 0.68 | 0.62 | 0.65 | 0.75 | 0.68 |
| $(V_{test}/V_{pred})_{5\%}$ | 0.79 | 0.71 | 0.91 | 0.80 | 0.97 | 0.85 | 0.92 | 0.80 |
| Maximum | 2.26 | 2.40 | 2.28 | 1.84 | 5.53 | 2.34 | 2.20 | 1.73 |
| $(V_{test}/V_{pred})_{95\%}$ | 1.53 | 1.90 | 1.62 | 1.38 | 2.77 | 1.65 | 1.60 | 1.28 |

*Table 2 Mari et al. (2014)*

| | | 892 beams without stirrups | | | | | | | | | 239 beams with stirrups | | | | | | | | |
|---|---|---|---|---|---|---|---|---|---|---|---|---|---|---|---|---|---|---|---|
| | | | EC-2 | | ACI318-08 | | MC10 Lev II | | Proposal | | | EC-2 | | ACI318-08 | | MC10 Lev III | | Proposal | |
| Criterion | | # | Mean | COV | Mean | COV | Mean | COV | Mean | COV | # | Mean | COV | Mean | COV | Mean | COV | Mean | COV |
| All | | 892 | 1.07 | 21.12 | 1.28 | 27.11 | 1.20 | 18.61 | 1.04 | **17.28** | 239 | 1.72 | 37.13 | 1.25 | 21.04 | 1.21 | 18.58 | 1.02 | **16.60** |
| $d$ (mm) | <300 | 665 | 1.10 | 21.08 | 1.38 | 22.11 | 1.23 | 18.57 | 1.03 | **18.07** | 117 | 1.89 | 39.63 | 1.38 | 17.60 | 1.33 | **16.79** | 1.05 | 17.66 |
| | 300–600 | 155 | 1.03 | 15.05 | 1.09 | 18.76 | 1.14 | 14.21 | 1.06 | **13.39** | 93 | 1.55 | 30.96 | 1.18 | 16.63 | 1.13 | **14.50** | 0.98 | 15.20 |
| | >600 | 72 | 0.86 | 18.30 | 0.71 | 26.41 | 1.02 | 15.79 | 1.06 | **17.36** | 29 | 1.58 | 25.51 | 0.94 | 17.74 | 1.00 | **11.85** | 1.03 | 12.63 |
| $f_c$ (MPa) | <40 | 626 | 1.06 | 18.94 | 1.29 | 25.31 | 1.18 | 16.41 | 1.04 | **15.68** | 111 | 1.73 | 44.51 | 1.23 | 18.86 | 1.20 | 16.99 | 1.01 | **14.93** |
| | 40–70 | 183 | 1.10 | 23.67 | 1.24 | 29.11 | 1.17 | 19.79 | 0.99 | **19.54** | 65 | 1.65 | 24.99 | 1.24 | 18.08 | 1.19 | 15.19 | 1.00 | **13.79** |
| | >70 | 83 | 1.09 | 28.31 | 1.29 | 34.86 | 1.40 | 21.23 | 1.10 | **20.99** | 63 | 1.78 | 32.45 | 1.29 | 26.20 | 1.27 | 22.92 | 1.07 | **20.48** |
| $\rho$ (%) | <1 | 139 | 0.94 | 16.05 | 0.88 | 26.50 | 1.16 | **13.21** | 0.99 | 14.29 | 7 | 1.34 | 16.65 | 1.04 | 26.13 | 1.24 | 21.80 | 1.12 | **9.24** |
| | 1–3 | 627 | 1.06 | 19.50 | 1.32 | 23.44 | 1.20 | 17.71 | 1.03 | **16.80** | 175 | 1.73 | 36.29 | 1.21 | 20.91 | 1.19 | 18.62 | 1.02 | **16.44** |
| | >3 | 126 | 1.24 | 22.00 | 1.50 | 18.95 | 1.30 | 21.66 | 1.05 | **17.59** | 57 | 1.72 | 40.15 | 1.38 | **17.46** | 1.27 | 17.61 | 1.02 | 17.77 |
| $\rho_w$ (MPa) | <0.70 | – | – | – | – | – | – | – | – | – | 130 | 1.95 | 34.49 | 1.17 | 20.31 | 1.18 | 17.23 | 0.99 | **15.03** |
| | 0.70–1.50 | – | – | – | – | – | – | – | – | – | 91 | 1.54 | 28.84 | 1.34 | 20.61 | 1.28 | 19.58 | 1.06 | **18.26** |
| | >1.50 | – | – | – | – | – | – | – | – | – | 18 | 0.97 | 28.12 | 1.28 | 14.46 | 1.14 | 15.38 | 1.04 | **13.11** |

*Table 3 Mari et al. (2014)*

As the effective depth of elements increase, the accuracy ($V_{test}/V_{pred}$) of the models (EC2, ACI, MC2010 and the proposed mode) do too. This could be due to the factor that all the models emphasise the the strength of the concrete more accuratley than the other elements in their respective model.

The accuracy of all the models were sensitive to the effective depth, d, of the beam. As the effective depth increases, the models tend to become less conservative. The EC-2 and the ACI 318-08 tends to overestimates the shear strength of beams with effective depths of more than 500 mm, which is unsafe. The EC-2 tends to be overly conservative for beams without stirrups and effective depths less than 500 mm, making for overcostly design. The accuracy of the proposed model's predictions is much less sensitive to variations in effective depth.

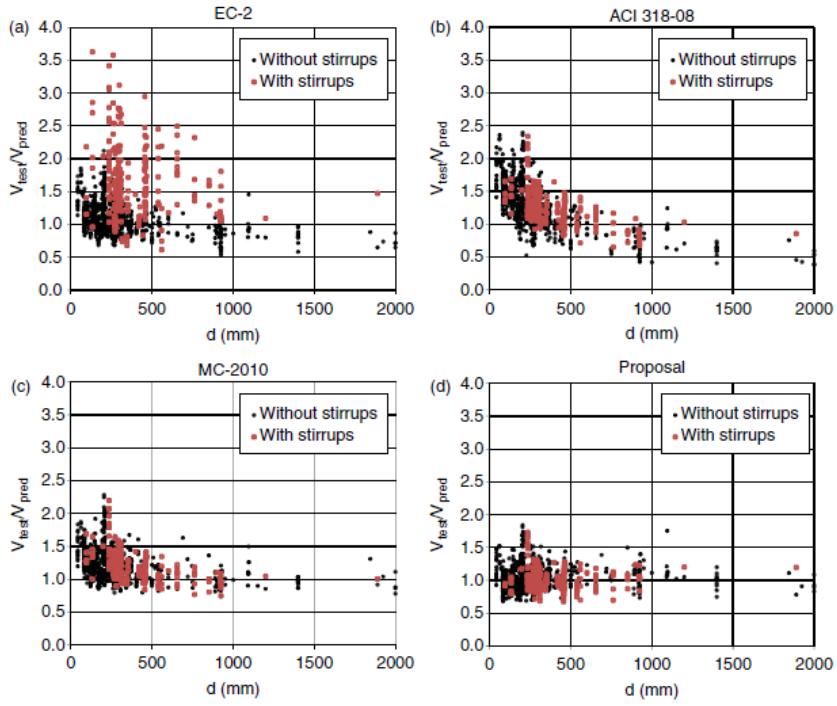


*Figure 27 Mari et al. (2014)*

The accuracy of the predictions of the models were sensitive to the amount of transverse reinforcement. The EC-2 was overly conservative, while the proposed model predictions fit well with the experimental resulsts and was largley unaffected by changes in the amount of transverse reinforcement. See figure 29.

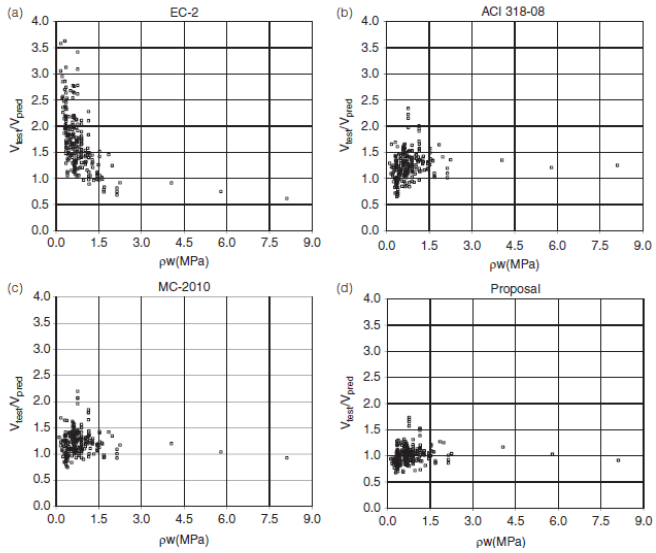


*Figure 28 Mari et al. (2014)*

# Chapter 4. Results and discussion

## 4.1 Data analysis

Using the procedures outlined in section 3.6 and 2.5, the predicted shear strengths of the 2 models were obtained and compared to the experimental results. All safety factors were removed from the design codes during calculations. The predicted shear strengths were plotted against the experimental shear forces. The results have been plotted in figure 30 and 31.Statistical analysis of the results are given in table 4, 5 and 6.

A database, compromised of a total of 121 beams, 43 beams with stirrups and 78 without stirrups were used to determine the accuracy of the 2 models. The accuracy of the test were predicted by plotting the experimental results against the predicted results.

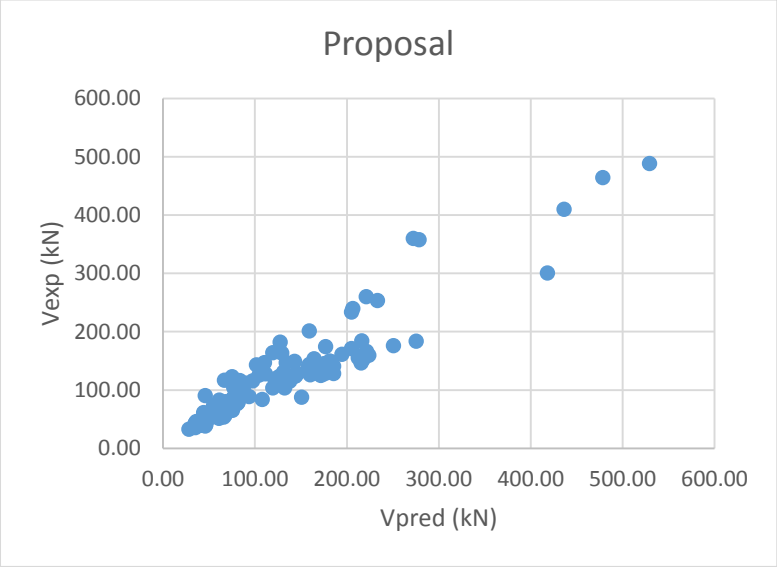


*Figure 29*

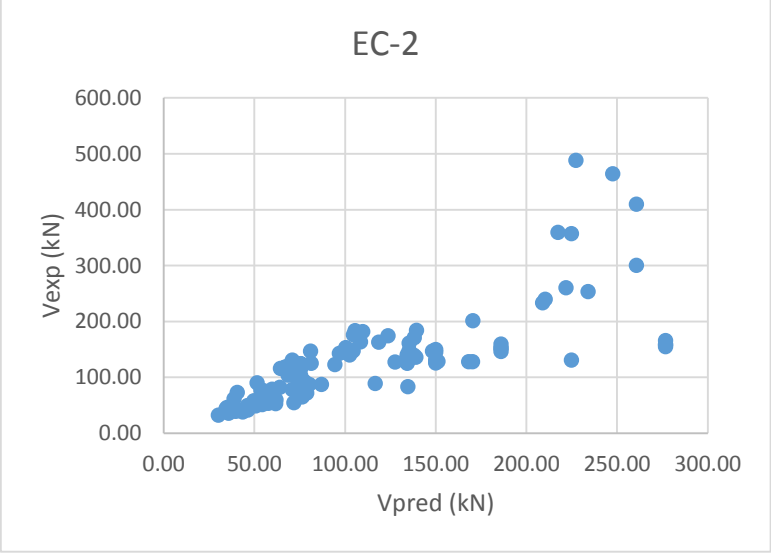


*Figure 30*

### 4.1.1 Beams without Stirrups

| Without Stirrups | EC-2 | Mari |
|---|---|---|
| Standard Deviation | 0.33 | 0.23 |
| Mean | 1.23 | 1.11 |
| COV | 0.26 | 0.20 |
| Sample Size | 78 | 78 |
| Max | 2.15 | 1.96 |
| Min | 0.62 | 0.67 |

*Table 4*

Both models tend to underestimate the shear strength of unreinforced beams, but the model proposed by Mari et al. (2014) underestimates the shear strength to a lesser degree.

The dispersion of the models are relatively low, but Mari's model performs better with a dispersion of 20% versus the 26% of the EC-2. This is in accord with the findings of Mari et al. (2014) and Sagaseta & Vollum (2010), who found the dispersion to be 21.2% and 21% for the EC-2 and 17.28% for the proposed model (Mari et al, 2014).

The COV both the models are good, but Mari's model is better. A certain amount of dispersion is to be expected, as random factors like the inclination of the shear crack affect the shear strength of the beam (Sagasete & Vollum, 2010).

### 4.1.2 Beams with Stirrups

| With Stirrups | EC-2 | Mari |
|---|---|---|
| Standard Deviation | 0.40 | 0.09 |
| Mean | 1.10 | 0.80 |
| COV | 0.36 | 0.12 |
| Sample Size | 43 | 43 |
| Max | 1.85 | 1.00 |
| Min | 0.56 | 0.58 |

*Table 5*

The models give very different predictions of the shear strength of beams with stirrups. The EC-2 is overly conservative and underestimates the shear strength, which is consistent with the findings of Sagasete & Vollum (2010). Because the EC-2 only considers the stirrups in the central ¾ of the shear span, this might explain why it overestimates shear strength of beams.

On the other hand, the proposed model overestimates the shear strength of beams. An explanation for this is that as the load approaches the support, the diagonal shear crack angles itself more towards the vertical, causing fewer stirrups to cross the crack.

The proposed model has a remarkably low COV of 11.6%, compared to the findings of Mari et al. (2014) of 16.60%. The dispersion of the EC-2 was found to be 36%. This is in accord with the results obtained by Mari et al. (2014) and Sagasete & Vollum (2010), who both calculated the dispersion to be 37%, using data bases of 239 and 47 beams respectively.

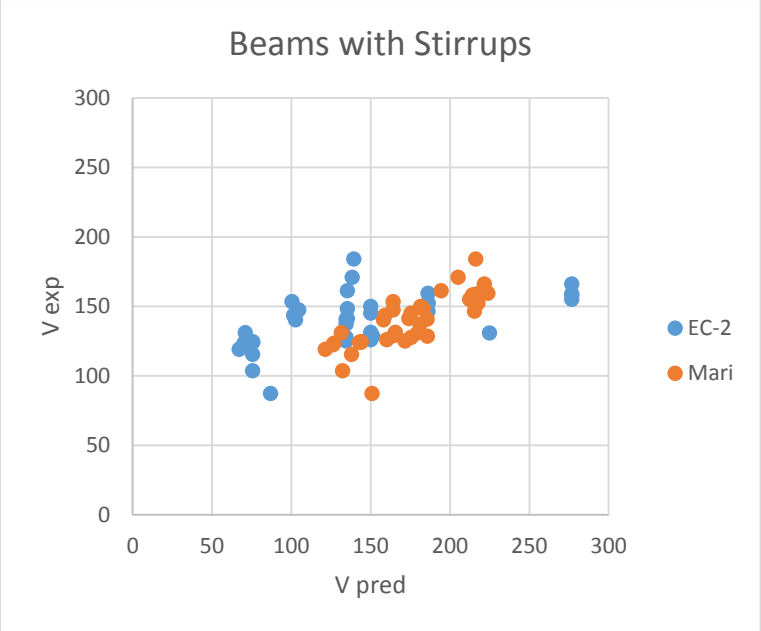


*Figure 31*

### 4.1.3 All beams

| All tests | EC-2 | Mari |
|---|---|---|
| **Standard Deviation** | **0.36** | **0.24** |
| **Mean** | **1.19** | **1.00** |
| **COV** | **0.30** | **0.24** |
| **Sample Size** | **121** | **121** |
| **Max** | **2.15** | **1.96** |
| **Min** | **0.56** | **0.58** |

*Table 6*

The mean prediction of the proposed model fit perfectly to the experimental models, but this is a reflection of the fact that it overestimates the shear strength of beams with stirrups, while underestimating the shear strength of beams without. This is reflected in the larger dispersion.

The EC-2 tends to underestimate the shear strength for all beams, and becomes more conservative as the magnitude of the total load increases, as seen from figure 33.

The EC-2 does not consider the shear strength enhancing effects of loads close to the shear crack, but the proposed model does. In addition, the EC-2 assumes plane section stresses, but Mari's model does not. These are major differences and likely contributors to the difference in results.

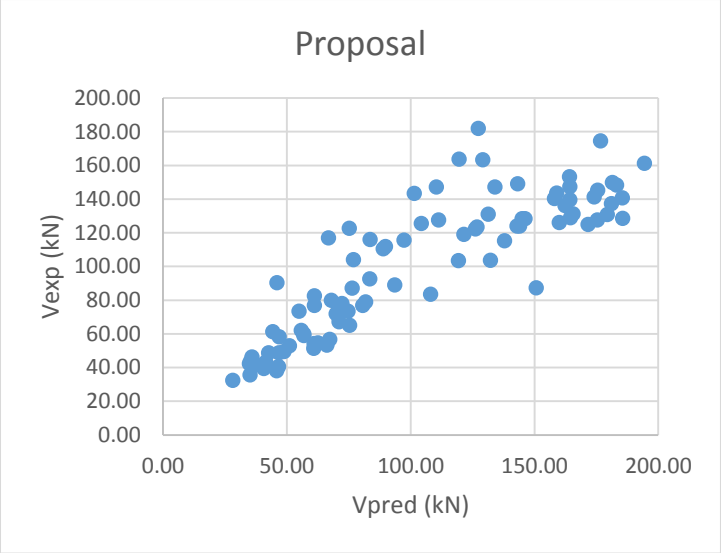


*Figure 32*

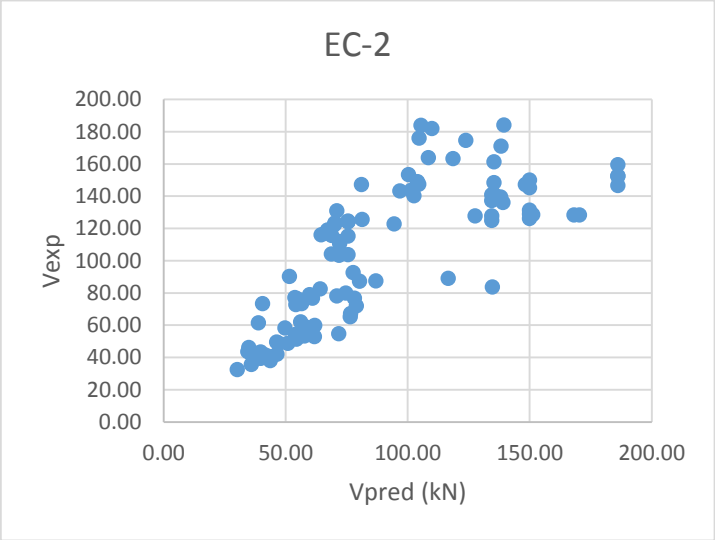


*Figure 33*

## 4.2 Parametric studies

The a/d-ratio, depth, longitudinal and transverse reinforcement ratios and the shear span were plotted against the accuracy of the models in order to investigate the influence of those parameters on the models.

### 4.2.1 Shear strength and a/d-ratio

From figure 35, it can be seen that as the a/d ratio decreases, the shear capacity of the beams increase. The reason for this is that as the shear arm decreases, the vertical crack increases in angle with respect to the horizontal. While this mean that the shear resistance of the reinforcement decreases due to less stirrups being active, it increases the shear strength of the concrete by vertical compression. Additionally, a direct strut that angles more to the horizontal is more capable to utilise it's the compressive strength of the concrete.

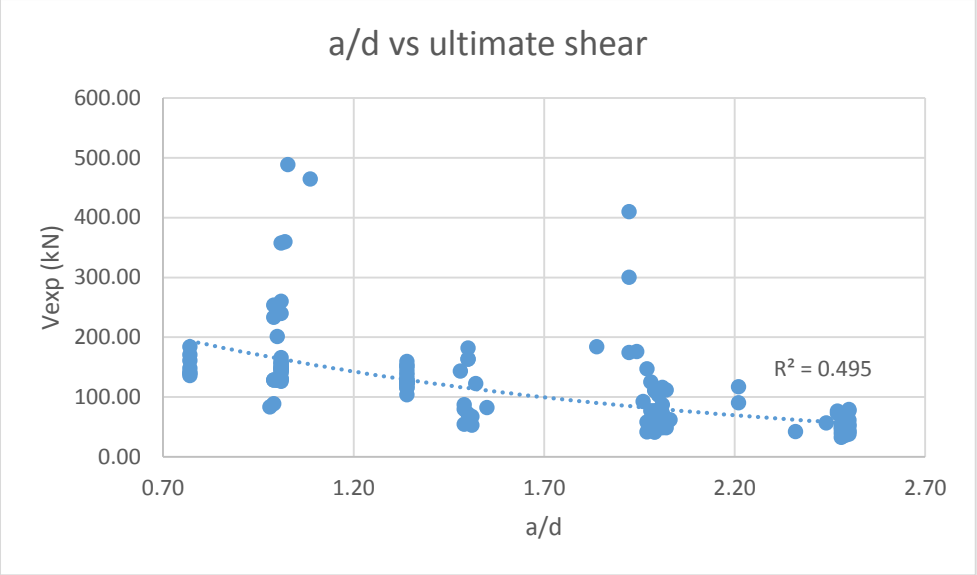


*Figure 34*

### 4.2.2 Accuracy and a/d-ratio

The accuracy of the predictions of the models are not affected by the a/d-ratio. The coefficients of determination are too low on both trend lines to conclude any correlation. This result for the EC-2 is in accord with results obtained by Sagaseta & Vollum (2010).

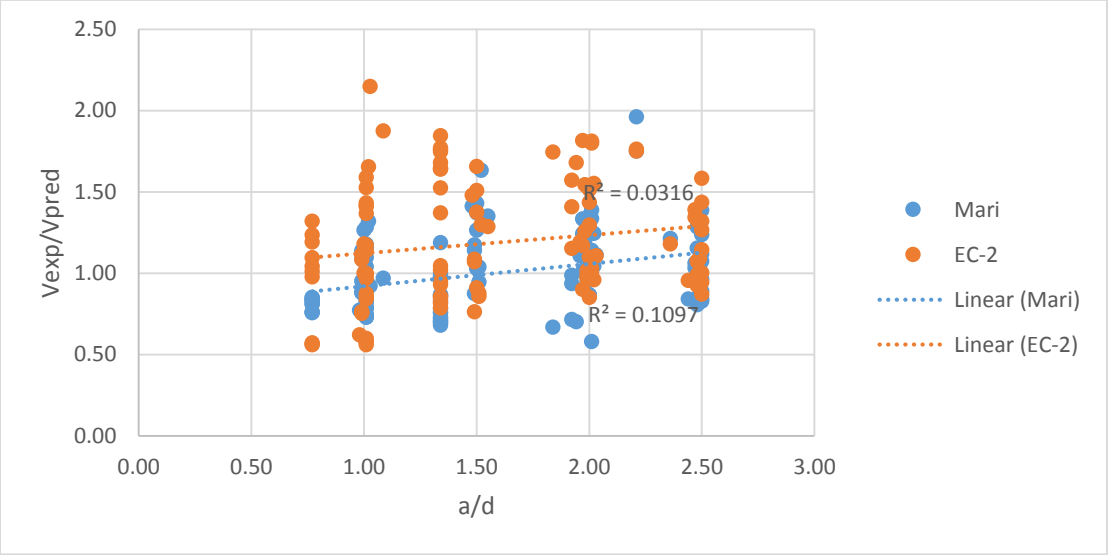


*Figure 35*

### 4.2.3 Accuracy and effective depth

As the trend lines in figure 37 have very low statistical validity, no correlation between depth and accuracy can be established with adequate certainty for either models.

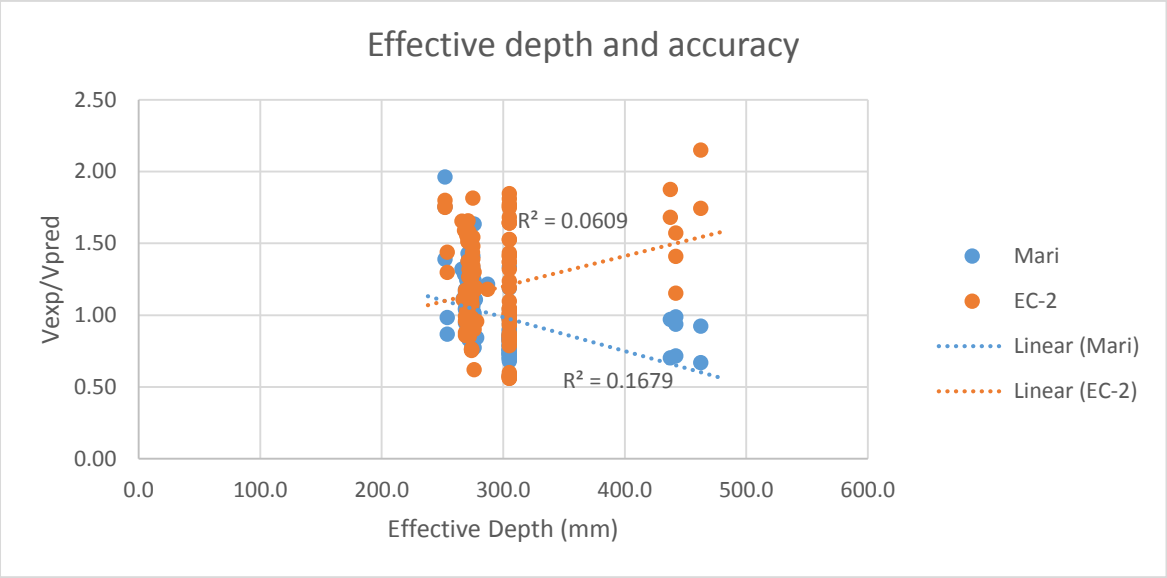


*Figure 36*

### 4.2.4 Accuracy and longitudinal reinforcement ratio

No correlation could be established between the longitudinal reinforcement ratio and the accuracy of the proposed model, see figure 38. A correlation was found for the EC-2, but the statistical validity is too flimsy to make any claim, see figure 39. Therefore it is concluded that the longitudinal reinforcement ratio has no effect on the accuracy of the predictions for either model.

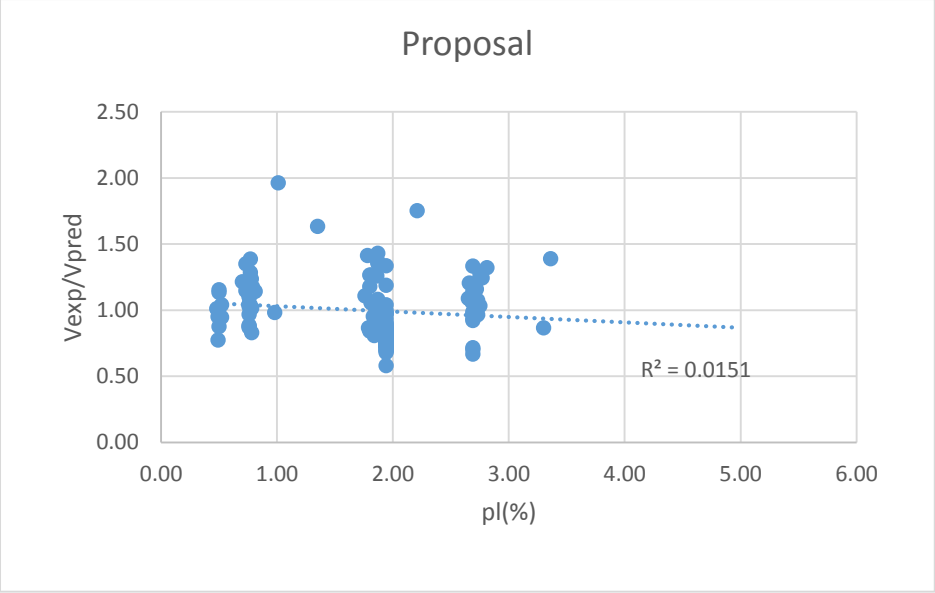


*Figure 37*

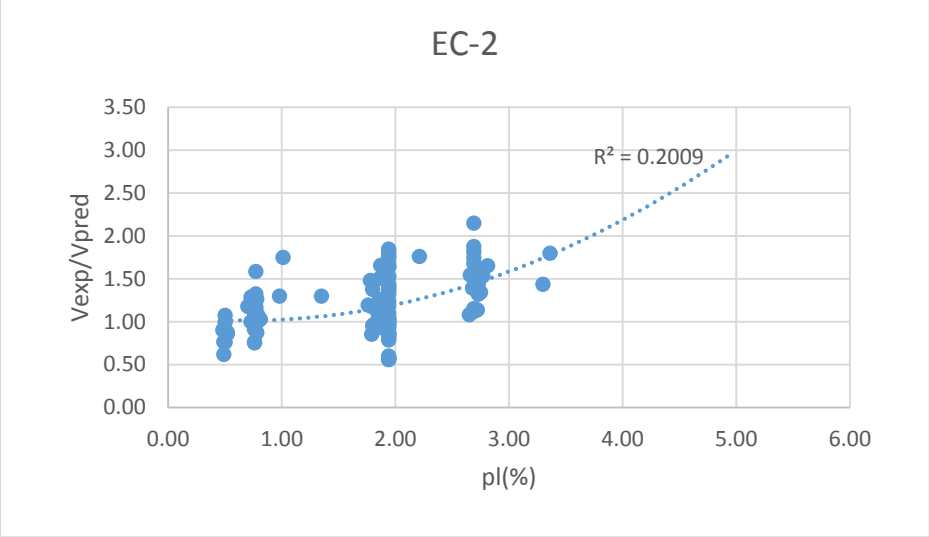


*Figure 38*

### 4.2.5 Accuracy and transverse reinforcement ratio

No statistical valid evidence was found to claim any correlation between the transverse reinforcement ratio and the accuracy of the models, see figure 40. The polynomial trend line shows that the first initial increases in transverse reinforcement from 0 increases the accuracy of the proposed model. While the correlation is low, this may indicate that Mari's model captures the effect of concrete confinement due to reinforcement.

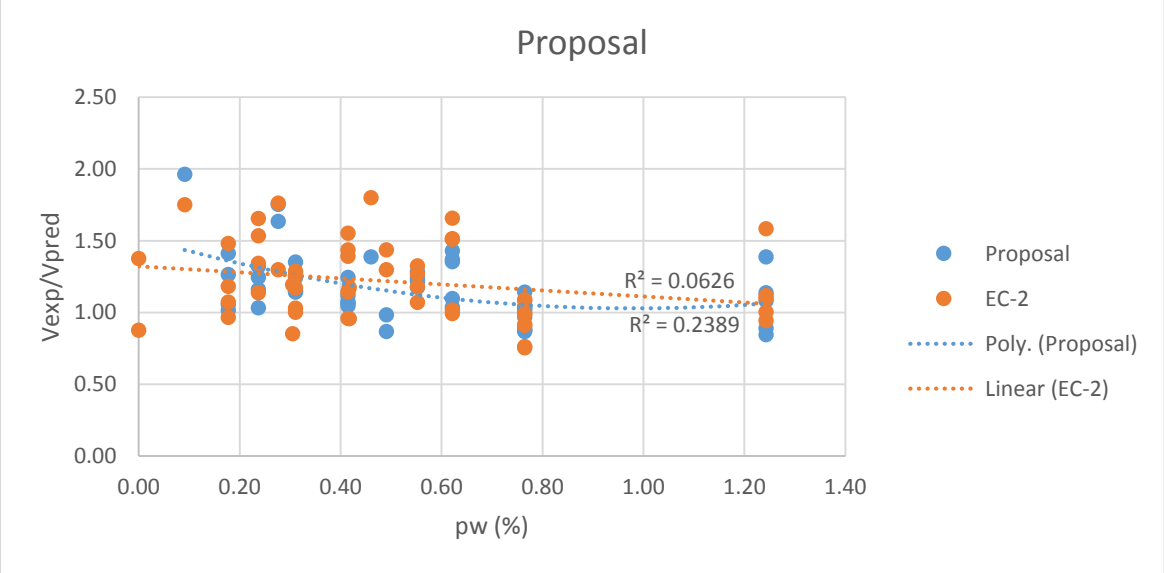


*Figure 39*

### 4.2.6 Accuracy and shear span

The shear span, a, does not have an effect on the accuracy of the proposed model's predictions or of the predictions of the EC-2, see figure 41.

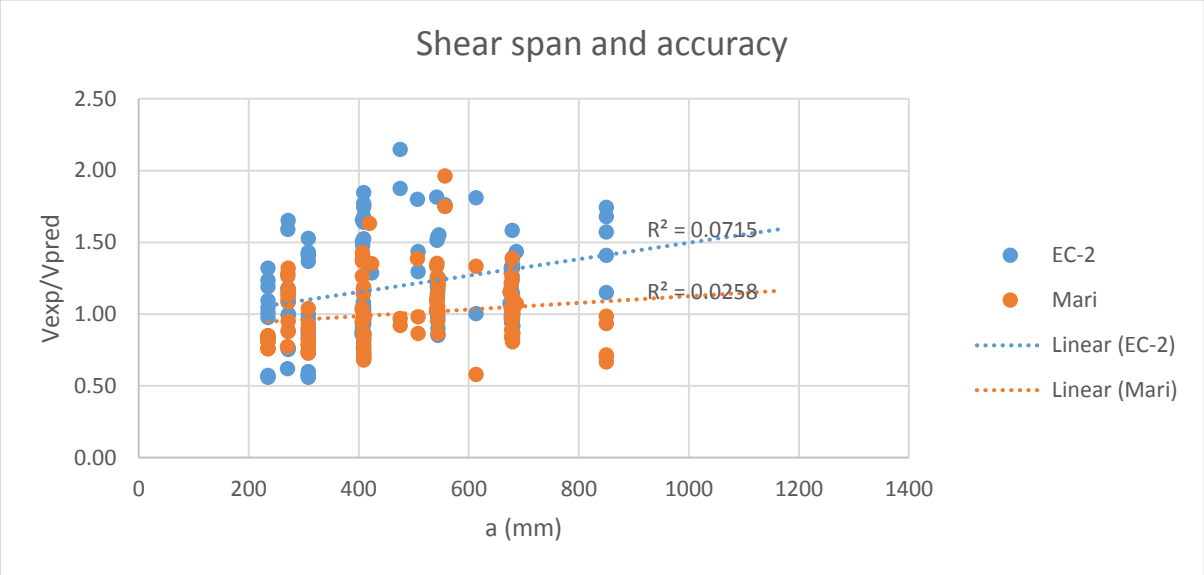


*Figure 40*

### 4.2.7 Parametric variation

There is a large range in the various parameters used to predict the shear strength of the beams. If a parameter range includes extreme values, a model might have difficulties capturing the effects of the extreme values accurately. The only extreme data found in the data base were very low longitudinal shear reinforcement ratios. While the accuracy of both models are unaffected by any single parameter listed in table 7, the proposed model as managed to account for the total effect of all the parameters.

| | $V_{exp}$ (kN) | d (mm) | a/d | a (mm) | $\rho_w$ (%) | $\rho_l$ (%) | fck (MPa) |
|---|---|---|---|---|---|---|---|
| **Max** | **634.3** | **483.0** | **2.50** | **1168.9** | **0.76** | **4.93** | **45.7** |
| **Min** | **32.5** | **238.0** | **0.77** | **234.9** | **0.18** | **0.48** | **12.3** |

*Table 7*

When investigating the effect of a single parameter, ideally, all the other parameters should remain constant. This is not the case for the data used in this paper. This further makes it harder to make any claim with certainty. The coefficients of variation might not have successfully account for this, and the correlations establish may be different from what they state.

## 4.3 Finite element model

The second assumption of the proposed model is that vertical stresses are bilinear, distributed as seen in figure 14. In order to test the assumption that that the vertical stresses in the beam are distributed in that manner, a finite element model was generated to investigate.

The generated 2D model was based on beam S1-1 from “Shear reinforcement in RC beams with multiple point loads” published by Vollum & Fang (2014), using the material properties, reinforcement detail and dimension of beam specified therein.

Whether intentional or not, the concrete covers surrounding the reinforcement is not constant. The concrete cover at the bottom and sides of the beam is only 17 mm, as the H8 reinforcement curves on the outside of the bottom longitudinal reinforcement. Thus less than the minimum nominal cover required in the EC-2. The concrete cover at the top of the beam is 27.5 mm.

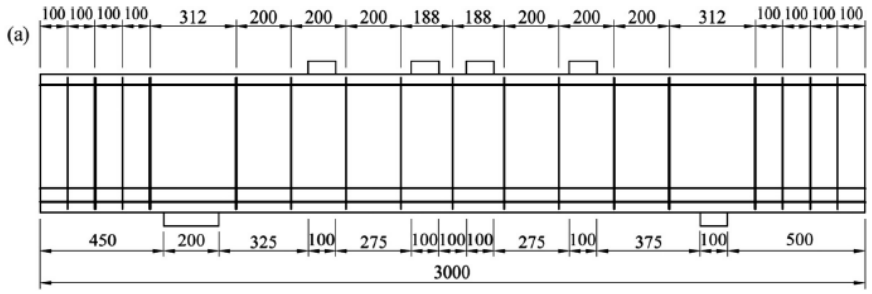


*Figure 41 Vollum & Fang (2014)*

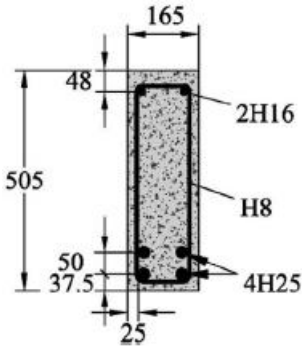


*Figure 42 Vollum & Fang (2014)*

### 4.3.1 Geometry and meshing

The main concrete body was meshed into elements 25mm wide and 25.5 mm high. The loading and support plates of the beam were 50 mm high, and while the loading plate was 150 mm long, the support plates where 200 and 100 mm long (left and right respectively). The plates were meshed into elements 25 by 25 mm long. The reinforcement was drawn as 1D lines and assigned the correct properties.

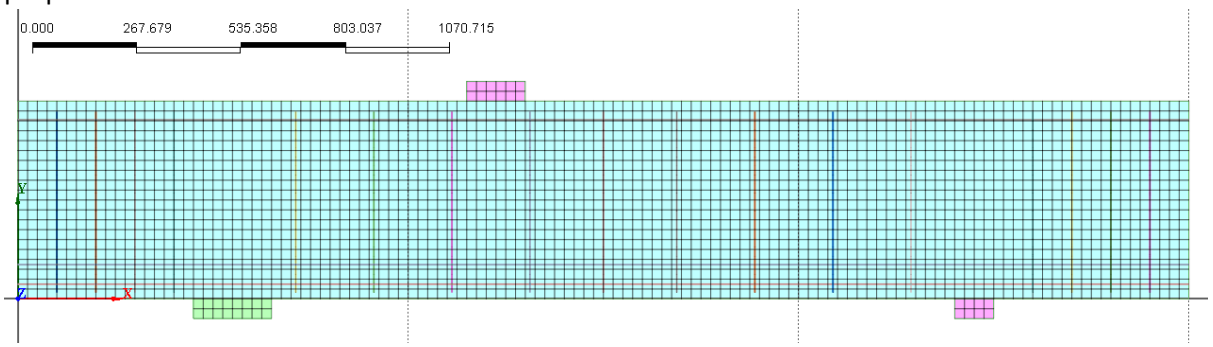


*Figure 43*

### 4.3.2 Materials and properties

In Vollum’s research, the bearing and loading plates were bedded on to the beam with a thin layer of mortar. The loading plates were therefor assigned the same properties as the concrete. Three different material properties were used for the 3 types of reinforcement, matching what was used in Vollum’s experiments. The material properties are listed in table 8, below. The width of the bearing plates, loading plates and the concrete was set to 165 mm.

| Material | E (MPa) | Weight (N/mm$^3$) | Poisson's Ratio, v | Model Type |
|---|---|---|---|---|
| Concrete | 35600 | 0.000025 | 0.2 | Elastic |
| H8 Reinforcement | 200000 | 0.000075 | 0.3 | Elastic |
| H16 Reinforcement | 200000 | 0.000075 | 0.3 | Elastic |
| H25 Reinforcement | 200000 | 0.000075 | 0.3 | Elastic |
| Loading and bearing plates | 35600 | 0.000025 | 0.2 | Elastic |

*Table 8*

### 4.3.3 Loading

The effect of a single load was modelled, where the centre of the load was placed at a distance a/d = 1, 1.5, and 2 from the centre of the support. In order to make the model work properly, this distances was fudged in order for the nodes to align. So the exact a/d-ratios are 1.018, 1.527, 1.980 This gave $a_v$ = 275, 500, 700 and a = 440, 675 and 875 respectively.

The load was applied as a pressure acting on the loading plate. The total pressure applied was 25000 N, but it was distributed across the entire loading plate, acting as an edge pressure of 166.7 N/mm$^2$. This equals the load applied at failure in the experiment.

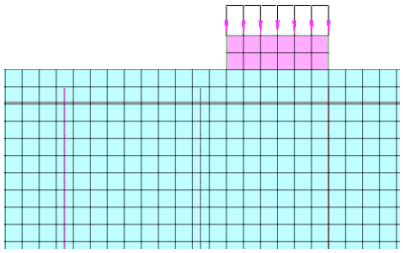

*Figure 44*

### 4.3.4 Constraints

All the bottom nodes of the supports were constrained against displacement in the y and z directions. Additionally, the central node at the left support is also constrained in the x-direction.

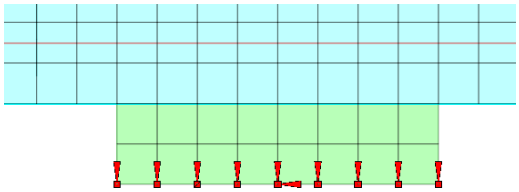

*Figure 45*

### 4.3.5 Model validity

The model functions well, and compressive stresses can be seen accumulating under the loading plate and at the supports, see figure 47. The reactions at the support are tensile and compressive, with the compressive stresses closest to the load. Analysis of the reactions at the loads show that the beam is in static equilibrium, indicating that the model is correctly computed.

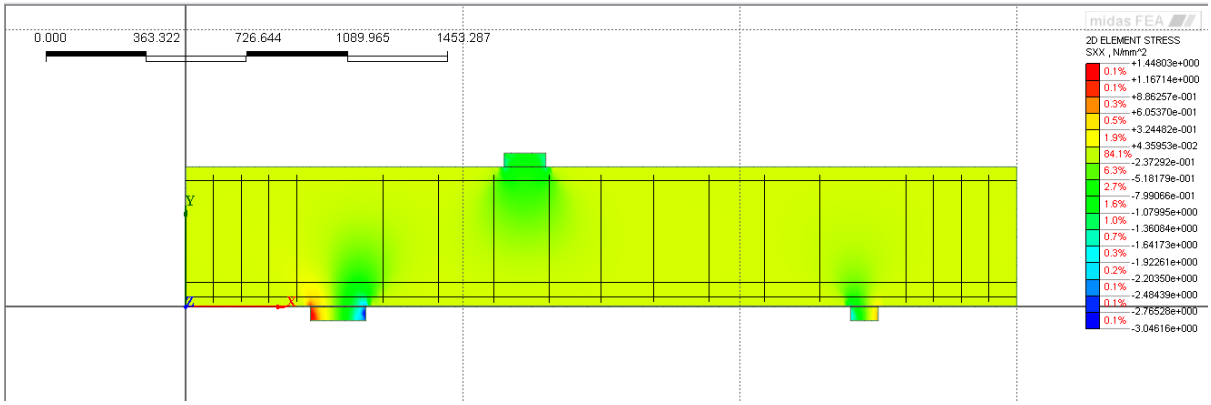


*Figure 46*

### 4.3.6 Finite element model results

Figure 48, 49 and 50 show the vertical stresses distributed throughout the beam. For clarity, only compressive stresses between up to 2 N/mm$^2$ have been shown.

a/d=2

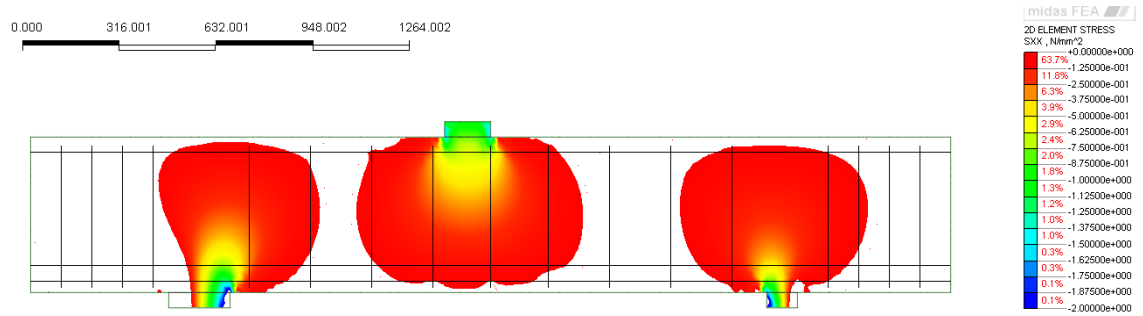


*Figure 47*

a/d=1.5

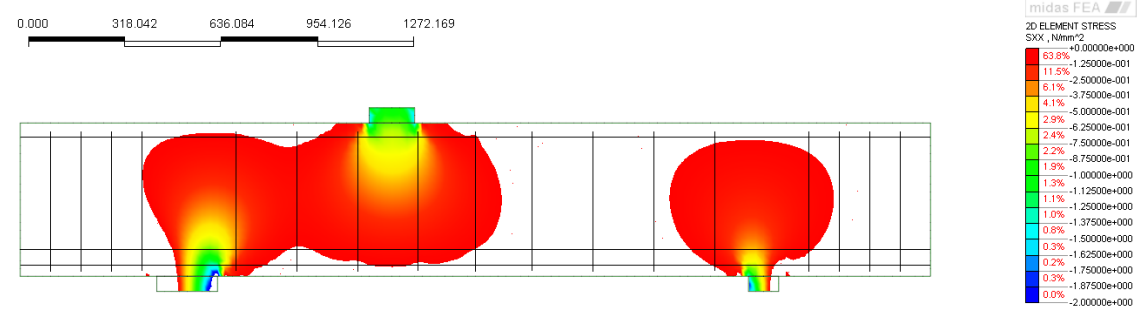


*Figure 48*

a/d=1

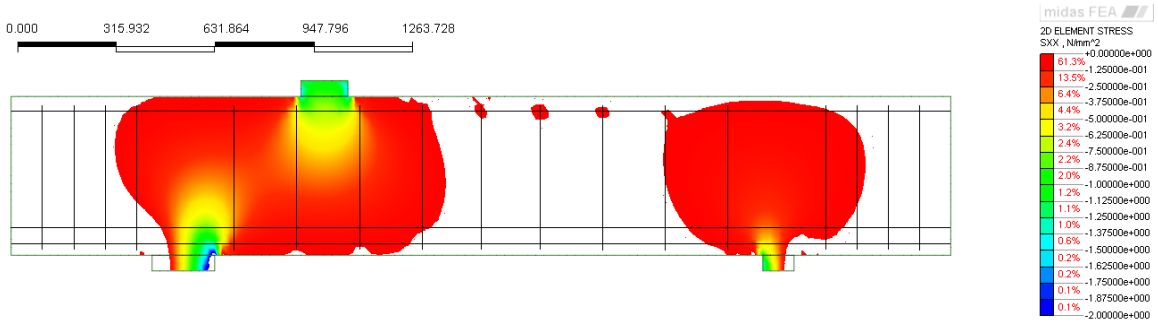


*Figure 49*

### 4.3.7 Distribution of vertical load

A horizontal cut was made at the neutral axis of the b-zone, showing the vertical stresses along the neutral axis. As expected, the largest concentrations of vertical stresses were found directly under the load. This stress decreases almost linearly as one moves along the cut, away from the edge of the load plate.

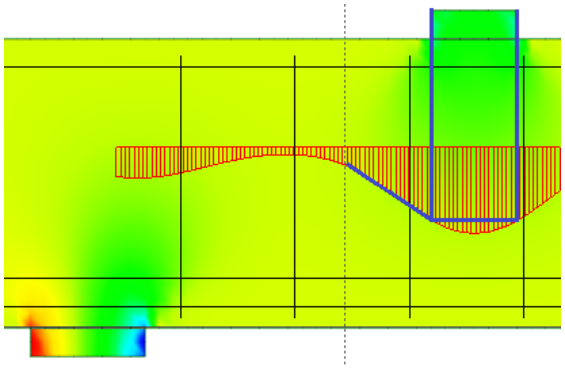

*Figure 50*

Sectional analysis of vertical stresses close to the support confirms the assumption made by Mari et al. (2014). Where the load is 0 at the top fibre, the vertical stresses increase linearly until it reaches the y-section. However, this relationship breaks down when the section is placed too close to the support, where the maximum shear stress tends to peak before the y-section. In the area very close to the support, the model shows vertical stresses in the top fibres. This is unexpected and can indicate a minor problem with the model. But as this only extends for a short distance from the load, the model is considered fully functional.

Section 1

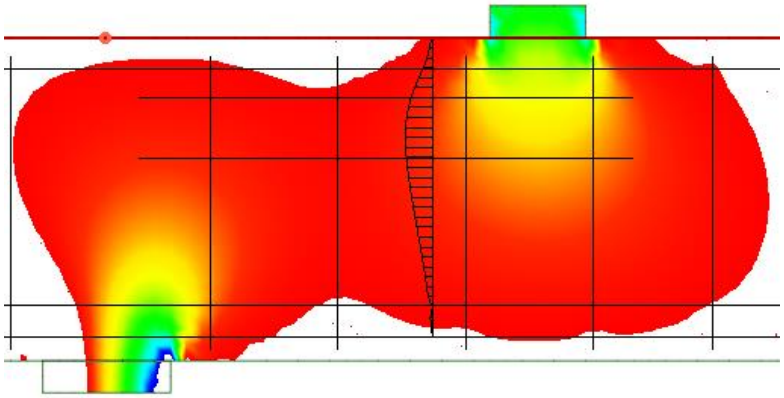

*Figure 51*

*Section 2*

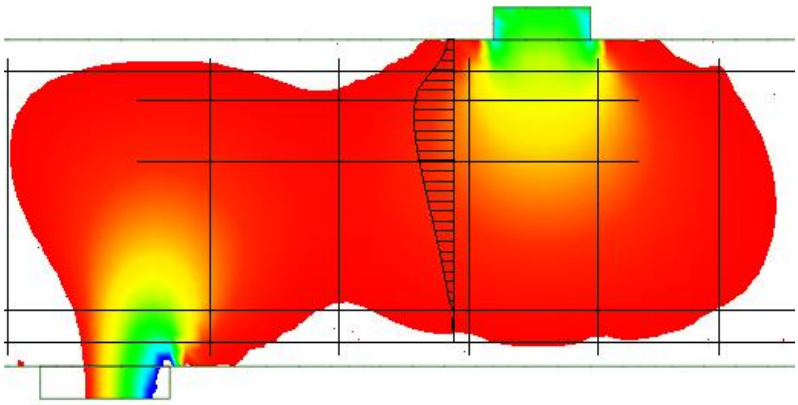

*Figure 52*

*Section 3*

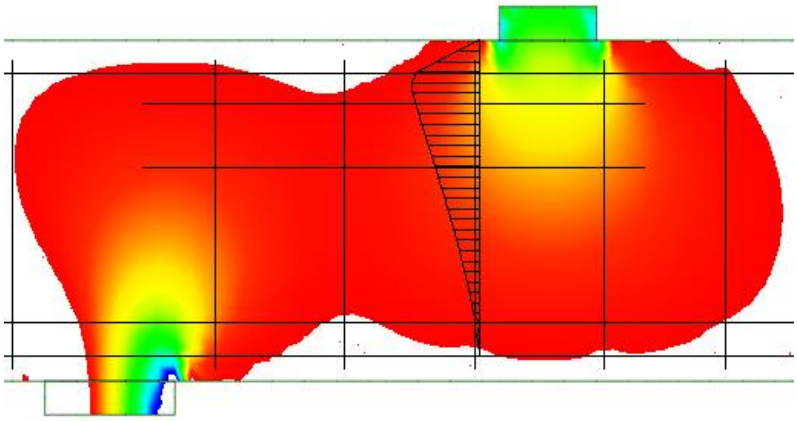

Figure 53

The ratio of vertical stresses between the y-section and the neutral axis, $\sigma_{xy}$-ratio vary with the distance from the load. The $\sigma_{xy}$-ratio is equal to the vertical stress at the y-section over the vertical stress at the neutral axis. Figure 55 below show the y-section and the neutral axis, in light and dark blue, respectively.

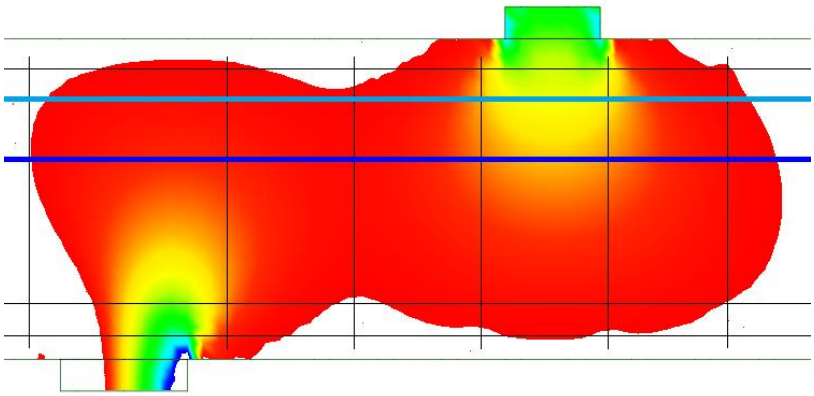

*Figure 54*

The $\sigma_{xy}$-ratio was plotted in figure 56. From that figure, it can be seen that the $\sigma_{xy}$-ratio varies between 1.67 and 0.29. Mari et al (2014) assumed that the $\sigma_{xy}$-ratio is constantly 1, which is only valid for a small section of the beam. It is close to 1 in a part of the beam, but this area is limited.

This discrepancy can be explained by the fact that Mari et al. (2014) assumes that the area between the y-axis and the neutral axis is a d-region, where plan section stress cannot be assumed. The solution of the model is based on a linear analysis, where plane section stresses are assumed. Therefore, the models prediction of the $\sigma_{xy}$-ratio can be considered invalid for the purpose of disproving the assumption. A non-linear analysis of the 2D beam would be required to validate that assumption.

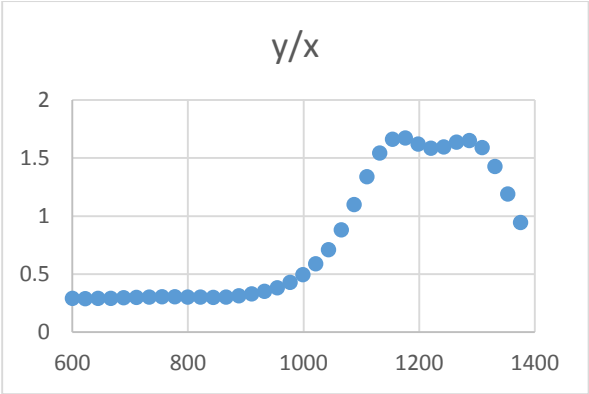


*Figure 55*

# Chapter 5. Conclusions and further research

## 5.1 Conclusions

The predictions of the EC-2 and the model proposed by Mari et al. (2014) have been compared, using a database of 121 beams to determine which model is the best predictor of shear strength in beams. 43 of the beams were reinforced by stirrups of different dimensions and 78 of the beams were without any reinforcement. Additional, a finite element model has been generated in order to investigate some of the assumptions made in the proposed model. The results allow the following conclusions to be made.

1) As the a/d-ratio becomes less than 2.5, the shear strength of beams tend to increase. This is because lowering this ratio enhances the shear strength of the concrete.

2) The causes for the increases in shear strength, according to the proposed model, come from two factors:

    3.1-1. As the a/d ratio is decreased below 2.5, the load gets closer to the critical section. This allows the local vertical stresses due to the load to act closer to the critical shear crack. These vertical stresses compress the crack, increasing aggregate friction and thus increasing the shear capacity of the crack in the concrete chord.

    3.1-2. As a/d becomes less than 2, failure occurs in the d-region where plane section stresses cannot be assumed. Compressive strength of the concrete chord can therefore be considered to be much higher than if the failure occurred in the b-region, where plane section stresses would be assumed instead.

3) The shear crack that develops is diagonal and occurs between the inner edges of the bearing and loading plates. As the load approaches the support, the diagonal crack angles itself more vertically, causing less reinforcement to cross the crack. Because of this, the shear capacity of the steel is reduced.

4) The proposed model assumes that failure occurs in the D-region. However, this can be adapted for cases where failure occurs within B-regions by increasing the depth of the neutral axis, which is a function of a/d and the vertical compressive stress induced by the load(s).

5) A working finite element model has be generated in order to investigate to of the assumptions made in the model. The first assumption, that the vertical stresses are 0 at the top fibre and increase linearly to the middle of the concrete chord at y=0.5 x is found to be true.

    The model did not confirm the assumption that vertical stresses remain constant between the y-axis and the neutral axis. Results showed differences in vertical stresses as one moved along the beam. However, these results are obtained using linear analysis of the section, which can be considered to be inapplicable, as the key area are considered to be within the d-region.

6) The EC-2 and the model proposed by Mari et al. (2014) has been compared to each other, using a database of 121 beams. The proposed model's mean predictions are 0.80 and 1.11 for beams with and without stirrups. The respective dispersions on the predictions are 11.6% and 20.4%. The EC-2's mean predictions were 1.10 and 1.23 for beams with and without stirrups, with respective dispersions of 36% and 26.4%.

   The proposed model compared favourably against the EC-2 for beams with and without stirrups. However, it has a tendency to overestimate the shear strength of reinforced beams, which is dangerous.

7) The parametric studies undertaken show that neither the effective depth, a/d-ratio, shear span, longitudinal reinforcement ratio nor the transverse reinforcement ratio had any effect on the accuracy of the predictions of either model. This implies that both models have captured the effect of these values well.

## 5.2 Future research

The EC-2 allows the use of a strut and tie model for design of short-span beams. Results obtained by Sagaseta & Vollum (2010) found that the mean prediction of this model ($V_{exp}/V_{pred}$) was 0.90 and 0.79 for beams with and without stirrups. The associated COV were 0.11 and 0.26, which are better results than that of the predicted model. For future analysis, a comparison between these two models, would elucidate which is the more preferable model.

A 2D non-linear analysis would take into account the cracking and non-linear stresses and strains assumed in the model. With such a model, the assumptions in the proposed model can be examined with more certainty.

The proposed model overestimates the shear strength of beams with stirrups. A detailed into the contribution of the stirrups can lead to results which can remedy this problem.

# References


ACI Committee 318. (2008). Building code requirements for structural concrete (ACI 318-08) and commentary. Farmington Hills, MI: American Concrete Institute.

ASTM C469-02ε1, "Standard Test Method for Static Modulus of Elasticity and Poisson's Ratio of Concrete in Compression," ASTM, West Conshohocken, PA, 2002, 5 pp.

Bentz, E. (2010). MC2010: Shear strength of beams and implications of the new approaches. Fib Bulletin 57: Shear and Punching Shear in RC and FRC Elements, Salo` (Italy). fib Bulletin, 57, 15–30.

Choi, K.K., Park, H.G., & Wight, J.K. (2007). Unified shear strength model for reinforced concrete beams - Part I: Development. ACI Structural Journal, 104, 142–152.

Collins, M.P., Bentz, E.C., & Sherwood, E.G. (2008). Where is shear reinforcement required? Review of research results and design procedures. ACI Structural Journal, 105, 590–600.

Cossio, R. De & Siess, C., 1960, Behavior and strength in shear of beams and frames without web reinforcement. ACIJournal Proceedings, (56), pp.695-736

Desai, S.B. (2004). Influence of constituents of concrete on its tensile strength and shear strength. ACI Structural Journal, 101, 29–38.

European Committee for Standardization (CEN). (2002). Eurocode 2: Design of concrete structures: Part 1: General rules and rules for buildings, Brussels, Belgium.

Fédération Internationale du Béton (fib) Task Group 8.2. (2008). Constitutive modelling of high strength/high performance concrete, fib Bulletin 42. Lausanne, Switzerland: Fédération Internationale du Béton.

Fédération Internationale du Béton (2013). fib Model Code for Concrete Structures 2010, Lausanne, Switzerland: Ernst & Sohn.

Jeong, J-P and Kim, W. (2014). Shear Resistant Mechanism into Base Components: Beam Action and Arch Action in Shear-Critical RC Members, International Journal of Concrete Structures and Materials, Vol.8, No.1, pp.1–14

Joint ACI-ASCE Committee 426, "Shear Strength of Reinforced Concrete Members (ACI 426R-74)," *Proceedings*, ASCE, V. 99, No. ST6, June 1973, pp. 1148-1157.

Kani, G., 1966. Basic facts concerning shear failure. ACI Journal Proceedings, 63(63), pp.675-692

Kani, G., 1967. How safe are our large reinforced concrete beams?. ACI Journal Proceedings, 64(64), pp.128-141

Khuntia, M., & Stojadinovic, B. (2001). Shear strength of reinforced concrete beams without transverse reinforcement. ACI Structural Journal, 98, 648–656.

Kotsovos, M.D., Bobrowski, J., & Eibl, J. (1987). Behaviour of reinforced concrete T-beams in shear. Structural Engineer, Part B: R&D Quarterly, 65 B(1), 1–10.

Krefeld, W. & Thurston, C., 1966. Studies of the shear and diagonal tension strength of simply supported reinforced concrete beams. ACI Journal of Proceedings (63)

KUPFER, H and Hilsdorf , H. K., Rusch, H. (1969). Behavior of Concrete Under Biaxial Stresses ACI JOURNAL No. 66-52, pp.656-666

Muttoni, A. (2008). Punching shear strength of reinforced concrete slabs without transverse reinforcement. ACI Structural Journal, 105, 440–450.

Muttoni, A., & Ruiz, M.F. (2008). Shear strength of members without transverse reinforcement as function of critical shear crack width. ACI Structural Journal, 105, 163–172.

Nakamura, E., Avendaño, A.R. & Bayrak, O., 2013. Shear Database for Prestressed Concrete Members, ACI Structural Journal, (110), pp.909-918

Park, H.G., Choi, K.K., & Wight, J.K. (2006). Strain-based shear strength model for slender beams without web reinforcement. ACI Structural Journal, 103, 783–793.

Park, H.G., Kang, S., & Choi, K.K. (2013). Analytical model for shear strength of ordinary and prestressed concrete beams. Engineering Structures, 46, 94–103. doi:10.1016/j.engstruct. 2012.07.015

Petrangeli, M., Pinto, P.E., & Ciampi, V. (1999). Fiber element for cyclic bending and shear of RC structures. I: Theory. Journal of Engineering Mechanics, 125, 994–1001. doi:10. 1061/(ASCE)0733-9399(1999)125:9(994)

Reineck, K., Kuchma, D.A., Kim, K.S., & Marx, S. (2003). Shear database for reinforced concrete members without shear reinforcement. ACI Structural Journal, 100, 240–249.

Reineck, K. (1991). Ultimate shear force of structural concrete members without transverse reinforcement derived from a mechanical model. ACI Structural Journal, 88, 592–602.

Ruddle, M.E., Rankin, G.I.B., & Long, A.E. (1999). Mohr approach to prediction of beam shear strength. Proceedings of the Institution of Civil Engineers: Structures and Buildings, 134, 363–372.

Sagaseta, J., & Vollum, R.L. (2010). Shear design of short-span beams. Magazine of Concrete Research, 62, pp.267–282.

Sagaseta, J., & Vollum, R.L. (2011). Influence of beam crosssection, loading arrangement and aggregate type on shear strength. Magazine of Concrete Research, 63, 139–155. http://infoscience.epfl.ch/record/163648/files/Sagaseta11.pdf

Smith, K.N. & Vantsiotis, a S., 1983. Shear strength of Deep Beams. ACI Journal, (79), pp.201-213

Tureyen, A.K., & Frosch, R.J. (2003). Concrete shear strength: Another perspective. ACI Structural Journal, 100, 609–615.

Tureyen, A.K., Wolf, T.S., & Frosch, R.J. (2006). Shear strength of reinforced concrete T-beams without transverse reinforcement. ACI Structural Journal, 103, 656–663.

Vecchio, F.J., & Collins, M.P. (1986). The modified compression- field theory for reinforced concrete elements subjected to shear. ACI Journal, 83, 219–231.

Vollum R. L. , Fang, L. (2014) Shear enhancement in RC beams with multiple point loads, Engineering Structures 80 (2014) 389–405

Wittmann, F. (2002). Crack formation and fracture energy of normal and high strength concrete. Sadhana, 27, 413–423.

Wolf, T.S., & Frosch, R.J. (2007). Shear design of prestressed concrete: A unified approach. Journal of Structural Engineering, 133, 1512–1519. doi:10.1061/(ASCE)0733- 9445(2007)133:11(1512)

Zanuy, C., Albajar, L., & Gallego, J.M. (2011). Toward modelling the shear fatigue behaviour of reinforced concrete beams without shear reinforcement. 7th International Conference on Analytical Models and New Concepts in Concrete and Masonry Structures AMCM, Krakow, Poland.

Zararis, P.D. (2003). Shear strength and minimum shear reinforcement of reinforced concrete slender beams. ACI Structural Journal, 100, 203–214.

Zararis, P.D., & Papadakis, G.C. (2001). Diagonal shear failure and size effect in RC beams without web reinforcement. Journal of Structural Engineering, 127, 733–742. doi:10.1061/(ASCE)0733-9445(2001)127:7(733)

# Annex A

The worked examples presented here are based on beam 3C1-20, found in Smith, K.N. & Vantsiotis, a S., 1983. Shear strength of Deep Beams. ACI Journal, (79), pp.201-213.

## Worked example, model proposed by Mari et al. (2014).

$\alpha_\varepsilon = E_s/E_c = 6.77$

$\rho_l = 0.019$

$\alpha_\varepsilon * \rho_l = 0.129$

Neutral axis in B-region:

$$\frac{x}{d} = \alpha_\varepsilon * \rho_l\left(-1 + \sqrt{1 + \frac{2}{\alpha_\varepsilon * \rho_l}}\right) = 0.40$$

Neutral axis in D-region:

$$\frac{x_1}{d} = \frac{x}{d} + \left(1 - \frac{x}{d}\right) * (1 - 0.4 * \frac{a_v}{d})^2 = 0.527$$

$X_1 = 160.87$ mm

Size effect factor:

$\zeta = 1.2-(0.2a) = 1.2 - (0.2*4087) = 1.12$ a in meters

Shear enhancement due to vertical loads:

$$\sigma_{cv} = \frac{0.85 * Q_d}{b(s_0 + \frac{a_v * x_1}{d})} = \frac{0.85 * Q_d}{b(s_0 + a_v * \frac{x_1}{d})} = \frac{0.85 * 140786\ N}{102\ mm * (101.6mm + 408.7mm * 0.527)}$$

$$\sigma_{cv} = 3.70$$

Angle of crack:

$$COT\theta = \frac{a_v}{d} < \frac{0.85 * d}{d - x_1}$$

$$COT\theta = \frac{408.7mm}{305\ mm} = 1.34 < \frac{0.85*305mm}{305\ mm - 161.3\ mm} = 1.804$$

Shear strength of steel:

$$V_{su} = \frac{A_{sw}}{s} f_{ywd}(d - x)\ sin\alpha\ (cot\theta + cot\alpha)$$

$$V_{su} = \frac{64.4\ mm^2}{114.3\ mm} * 437.5\ MPa * (305\ mm - 160.87\ \text{mm}) * 1.34 = 47607.6\ \text{N}$$

Shear strength of concrete:

$$V_{cu} = \zeta \frac{x}{d} K_p \left[ 0.30 \frac{f_{ck}^{\frac{2}{3}}}{\gamma_c} + \frac{V_{su}}{b \cdot d} + \sigma_{cv} \right] bd$$

$$V_{cu} = 1.12 * \ 0.527 * 1 \left[ 0.30 * \frac{21^{\frac{2}{3}} MPa}{1} + \frac{47607.6 \text{ N}}{102\ mm * 305\ mm} + 3.70\ MPa \right] * 102\ mm * 305\ mm$$

$$V_{cu} = 137894.1\ N$$

Total shear strength:

$V_u = V_{cu} + V_{su}$= 47564 N +137894 N =140.79 kN

Accuracy of prediction:

$V_{exp}$=140.79

$V_{exp}$ /$V_{pred}$=0.757

## Worked example, EC-2.

Shear capacity of concrete:

$$V_{Rd,c} = \ (C_{Rd,c} k (100 * \rho_l f_{ck})^{\frac{1}{3}} + k_1 \sigma_{cp}) b_w d$$

Size factor:

$k = (1 + \sqrt{\frac{200}{d}})$ = $(1 + \sqrt{\frac{200}{305\ mm}})$=1.81

$$V_{Rd,c} = \ 0.18 * 1.81 * (100 * 0.019 * 21MPa)^{\frac{1}{3}} + 0) * 102\ mm * 305\ mm$$

$$V_{Rd,c} = 34.8\ kN$$

Shear strength of steel:

Z = 0.9*d = 0.9 * 305 = 274.5 mm

$f_{ywd} = 437.5$

$cot\theta = \frac{a_v}{h} = \frac{307.1\ mm}{356\ mm}$=0.86

1 <cot θ< 2.5

cot θ = 1

$$V_{Rd,s} = \left( \frac{A_{sw}}{s} * z * f_{ywd} * cot\theta \right) = \left( \frac{64.4\ mm^2}{114.3\ mm} * 274.5\ mm * 437.5\ MPa * 1 \right) = 67.7\ kN$$

$V_{Rd,s,max} = (\frac{\alpha_{cw} * b_w * z * f_{cd} * v_1}{cot\theta + tan\theta})$

$v_1 = 0.6 * (1 - \frac{f_{ck}}{250})$ = $0.6 * (1 - \frac{21MPa}{250})$ = 0.55

Tan θ = 1.009

$V_{Rd,s,max} = (\frac{1 * 102\ mm * 274.5 * 0.85 * 21\ MPa * 0.55}{1 + 1.009})$ = 137.5

Total shear strength:

$V_{Rd} = Max\ (V_{Rd,c}, V_{Rd,s})$= 137.5

Accuracy of prediction:

$V_{exp}$ =140.5 kN

$$\frac{V_{exp}}{V_{pred}} = \frac{140.5}{137.5} = 1.05$$

# Annex B

Beam data base.

| Specimen Id | Vexp (kN) | Vpred EC2 (kN) | Vpred Mari (kN) | Vexp/Vpred EC | Vexp/Vpred Mari | d (mm) | a/d | a (mm) | ρw (%) | ρl (%) | fck (MPa) |
|---|---|---|---|---|---|---|---|---|---|---|---|
| Cossio & Siess, 1960 | | | | | | | | | | | |
| L-1 | 116.1 | 64.5 | 83.6 | 1.80 | 1.39 | 252.0 | 2.01 | 506.5 | 0.00 | 3.36 | 21.0 |
| A-1 | 73.4 | 56.6 | 74.7 | 1.30 | 0.98 | 254.0 | 2.00 | 508.0 | 0.00 | 0.98 | 28.1 |
| A-11 | 103.4 | 71.9 | 119.3 | 1.44 | 0.87 | 254.0 | 2.00 | 508.0 | 0.00 | 3.30 | 28.3 |
| D-14 | 90.3 | 51.6 | 46.0 | 1.75 | 1.96 | 252.0 | 2.21 | 556.9 | 0.00 | 1.01 | 32.1 |
| D-5 | 122.8 | 94.5 | 75.1 | 1.30 | 1.63 | 276.0 | 1.52 | 419.5 | 0.00 | 1.35 | 25.8 |
| D-4 | 117.0 | 66.4 | 66.8 | 1.76 | 1.75 | 252.0 | 2.21 | 556.9 | 0.00 | 2.21 | 34.6 |
| Kani ,1966, 1967 | | | | | | | | | | | |
| 23 | 163.8 | 108.5 | 119.5 | 1.51 | 1.37 | 271.0 | 1.50 | 406.5 | 0.00 | 1.87 | 26.9 |
| 24 | 182.0 | 109.9 | 127.3 | 1.66 | 1.43 | 271.0 | 1.50 | 406.5 | 0.00 | 1.87 | 27.9 |
| 25 | 104.1 | 68.7 | 76.9 | 1.52 | 1.35 | 271.0 | 2.00 | 542.0 | 0.00 | 1.87 | 24.6 |
| 26 | 78.1 | 71.0 | 72.2 | 1.10 | 1.08 | 271.0 | 2.00 | 542.0 | 0.00 | 1.87 | 27.1 |
| 27 | 51.4 | 54.4 | 60.8 | 0.94 | 0.84 | 271.0 | 2.50 | 677.5 | 0.00 | 1.88 | 29.8 |
| 28 | 54.3 | 54.0 | 60.9 | 1.00 | 0.89 | 271.0 | 2.50 | 677.5 | 0.00 | 1.88 | 29.2 |
| 85 | 233.6 | 208.9 | 205.1 | 1.12 | 1.14 | 274.0 | 0.99 | 271.3 | 0.00 | 2.69 | 25.5 |
| 87 | 239.6 | 210.5 | 206.6 | 1.14 | 1.16 | 269.0 | 1.01 | 271.7 | 0.00 | 2.72 | 27.2 |
| 88 | 359.8 | 217.5 | 272.4 | 1.65 | 1.32 | 266.0 | 1.02 | 271.3 | 0.00 | 2.81 | 31.4 |
| 94 | 110.6 | 72.1 | 88.9 | 1.53 | 1.24 | 273.0 | 1.99 | 543.3 | 0.00 | 2.77 | 25.3 |
| 95 | 72.8 | 54.2 | 70.5 | 1.34 | 1.03 | 275.0 | 2.47 | 679.3 | 0.00 | 2.75 | 25.3 |
| 98 | 76.3 | 54.8 | 71.8 | 1.39 | 1.06 | 275.0 | 2.47 | 679.3 | 0.00 | 2.68 | 26.2 |
| 99 | 77.2 | 53.7 | 71.8 | 1.44 | 1.07 | 274.6 | 2.50 | 686.5 | 0.00 | 2.73 | 26.2 |
| 100 | 111.9 | 72.0 | 89.9 | 1.55 | 1.25 | 270.0 | 2.02 | 545.4 | 0.00 | 2.75 | 27.2 |

| Specimen Id | Vexp (kN) | Vpred EC2 (kN) | Vpred Mari (kN) | Vexp/Vpred EC | Vexp/Vpred Mari | d (mm) | a/d | a (mm) | ρw (%) | ρl (%) | fck (MPa) |
|---|---|---|---|---|---|---|---|---|---|---|---|
| Kani ,1966, 1967 | | | | | | | | | | | |
| 102 | 48.8 | 50.9 | 46.7 | 0.96 | 1.05 | 269.0 | 2.02 | 543.4 | 0.00 | 0.76 | 25.3 |
| 105 | 41.5 | 36.3 | 37.1 | 1.14 | 1.12 | 271.8 | 2.50 | 679.5 | 0.00 | 0.77 | 21.2 |
| 108 | 147.1 | 148.2 | 134.0 | 0.99 | 1.10 | 269.0 | 1.01 | 271.7 | 0.00 | 0.76 | 25.0 |
| 109 | 71.9 | 79.0 | 69.9 | 0.91 | 1.03 | 271.0 | 1.50 | 406.5 | 0.00 | 0.76 | 25.0 |
| 111 | 43.3 | 39.7 | 41.5 | 1.09 | 1.04 | 272.0 | 2.49 | 677.3 | 0.00 | 0.76 | 27.0 |
| 112 | 39.4 | 39.8 | 40.7 | 0.99 | 0.97 | 273.0 | 2.48 | 677.0 | 0.00 | 0.76 | 27.0 |
| 113 | 87.2 | 80.3 | 76.4 | 1.09 | 1.14 | 274.0 | 1.49 | 408.3 | 0.00 | 0.77 | 25.5 |
| 115 | 61.4 | 38.8 | 44.3 | 1.58 | 1.39 | 271.5 | 2.50 | 678.8 | 0.00 | 0.77 | 26.2 |
| 127 | 201.4 | 170.5 | 159.2 | 1.18 | 1.27 | 271.0 | 1.00 | 271.0 | 0.00 | 1.81 | 15.7 |
| 129 | 143.3 | 96.8 | 101.4 | 1.48 | 1.41 | 275.0 | 1.48 | 407.0 | 0.00 | 1.78 | 17.6 |
| 131 | 49.6 | 46.3 | 48.8 | 1.07 | 1.02 | 274.0 | 2.48 | 679.5 | 0.00 | 1.85 | 18.1 |
| 134 | 59.9 | 62.0 | 56.8 | 0.97 | 1.05 | 273.0 | 1.99 | 543.3 | 0.00 | 1.81 | 17.4 |
| 135 | 76.8 | 61.0 | 61.1 | 1.26 | 1.26 | 274.0 | 1.98 | 542.5 | 0.00 | 1.86 | 17.4 |
| 141 | 48.7 | 47.2 | 42.7 | 1.03 | 1.14 | 270.0 | 2.01 | 542.7 | 0.00 | 0.81 | 19.3 |
| 142 | 58.3 | 49.8 | 46.9 | 1.17 | 1.24 | 276.0 | 1.97 | 543.7 | 0.00 | 0.77 | 19.3 |
| 145 | 82.5 | 64.1 | 61.1 | 1.29 | 1.35 | 273.0 | 1.55 | 423.2 | 0.00 | 0.73 | 16.2 |
| 146 | 127.7 | 127.6 | 111.3 | 1.00 | 1.15 | 272.0 | 1.00 | 272.0 | 0.00 | 0.73 | 16.2 |
| 147 | 42.3 | 35.8 | 34.8 | 1.18 | 1.21 | 287.0 | 2.36 | 677.3 | 0.00 | 0.70 | 16.8 |
| 148 | 79.9 | 74.6 | 68.0 | 1.07 | 1.17 | 274.0 | 1.49 | 408.3 | 0.00 | 0.79 | 19.9 |
| 149 | 43.7 | 34.5 | 35.3 | 1.27 | 1.24 | 271.5 | 2.50 | 678.8 | 0.00 | 0.78 | 18.0 |
| 150 | 46.2 | 34.9 | 35.9 | 1.32 | 1.29 | 273.0 | 2.48 | 677.0 | 0.00 | 0.77 | 18.0 |
| 151 | 35.6 | 35.9 | 35.1 | 0.99 | 1.01 | 273.0 | 2.49 | 679.8 | 0.00 | 0.78 | 19.3 |
| 162 | 59.0 | 58.0 | 56.8 | 1.02 | 1.04 | 272.0 | 1.99 | 541.3 | 0.00 | 0.77 | 34.3 |
| 163 | 40.5 | 44.1 | 46.6 | 0.92 | 0.87 | 273.0 | 2.49 | 679.8 | 0.00 | 0.76 | 35.4 |
| 167 | 128.4 | 170.4 | 146.1 | 0.75 | 0.88 | 274.0 | 0.99 | 271.3 | 0.00 | 0.76 | 36.4 |

| Specimen Id | Vexp (kN) | Vpred EC2 (kN) | Vpred Mari (kN) | Vexp/Vpred EC | Vexp/Vpred Mari | d (mm) | a/d | a (mm) | ρw (%) | ρl (%) | fck (MPa) |
|---|---|---|---|---|---|---|---|---|---|---|---|
| 169 | 128.4 | 168.2 | 145.0 | 0.76 | 0.89 | 274.0 | 0.99 | 271.3 | 0.00 | 0.76 | 36.4 |
| 178 | 67.2 | 76.6 | 71.0 | 0.88 | 0.95 | 269.0 | 1.51 | 406.2 | 0.00 | 0.52 | 34.5 |
| 181 | 65.2 | 76.5 | 75.3 | 0.85 | 0.87 | 272.0 | 2.00 | 544.0 | 0.00 | 1.79 | 33.9 |
| 183 | 260.3 | 221.9 | 220.9 | 1.17 | 1.18 | 269.0 | 1.01 | 271.7 | 0.00 | 1.80 | 35.4 |
| 184 | 163.3 | 118.6 | 129.1 | 1.38 | 1.26 | 271.0 | 1.50 | 406.5 | 0.00 | 1.80 | 35.1 |
| 188 | 92.6 | 77.6 | 83.5 | 1.19 | 1.11 | 277.0 | 1.96 | 542.9 | 0.00 | 1.76 | 33.1 |
| 193 | 56.7 | 59.3 | 67.3 | 0.96 | 0.84 | 278.0 | 2.44 | 678.3 | 0.00 | 1.80 | 34.6 |
| 197 | 53.4 | 57.7 | 66.1 | 0.92 | 0.81 | 274.0 | 2.48 | 679.5 | 0.00 | 1.84 | 36.0 |
| 199 | 76.8 | 78.2 | 80.6 | 0.98 | 0.95 | 273.0 | 1.99 | 543.3 | 0.00 | 1.83 | 36.0 |
| 201 | 253.7 | 234.1 | 233.2 | 1.08 | 1.09 | 274.0 | 0.99 | 271.3 | 0.00 | 2.65 | 35.2 |
| 203 | 357.6 | 224.9 | 278.5 | 1.59 | 1.28 | 268.0 | 1.01 | 270.7 | 0.00 | 2.75 | 34.8 |
| 204 | 147.1 | 81.0 | 110.3 | 1.82 | 1.33 | 275.0 | 1.97 | 541.8 | 0.00 | 2.69 | 34.8 |
| 205 | 125.5 | 81.3 | 104.2 | 1.54 | 1.20 | 275.0 | 1.98 | 544.5 | 0.00 | 2.66 | 35.2 |
| 210 | 79.0 | 59.8 | 81.8 | 1.32 | 0.96 | 271.8 | 2.50 | 679.5 | 0.00 | 2.73 | 35.2 |
| 249 | 83.6 | 134.7 | 108.0 | 0.62 | 0.77 | 276.0 | 0.98 | 270.5 | 0.00 | 0.49 | 28.0 |
| 250 | 54.7 | 71.8 | 62.5 | 0.76 | 0.88 | 274.0 | 1.49 | 408.3 | 0.00 | 0.50 | 28.0 |
| 251 | 41.9 | 46.5 | 41.4 | 0.90 | 1.01 | 276.0 | 1.97 | 543.7 | 0.00 | 0.48 | 26.2 |
| 265 | 53.0 | 61.7 | 51.0 | 0.86 | 1.04 | 269.0 | 1.51 | 406.2 | 0.00 | 0.52 | 18.1 |
| 266 | 32.5 | 30.2 | 28.2 | 1.08 | 1.15 | 272.0 | 2.48 | 674.6 | 0.00 | 0.50 | 18.1 |
| 269 | 89.0 | 116.6 | 93.5 | 0.76 | 0.95 | 274.0 | 0.99 | 271.3 | 0.00 | 0.49 | 18.1 |
| 270 | 41.4 | 41.8 | 36.5 | 0.99 | 1.14 | 273.0 | 1.99 | 543.3 | 0.00 | 0.50 | 20.1 |
| 162' | 62.1 | 56.1 | 55.8 | 1.11 | 1.11 | 267.0 | 2.03 | 541.9 | 0.00 | 0.76 | 34.3 |
| 163' | 38.0 | 43.6 | 45.9 | 0.87 | 0.83 | 271.8 | 2.50 | 679.5 | 0.00 | 0.78 | 35.4 |
| Smith & Vantsiotis, 1983 | | | | | | | | | | | |
| 0A0-44 | 139.5 | 138.1 | 164.3 | 1.01 | 0.85 | 305.0 | 0.77 | 234.9 | 0.00 | 1.94 | 20.5 |
| 0A0-48 | 136.1 | 139.1 | 162.3 | 0.98 | 0.84 | 305.0 | 0.77 | 234.9 | 0.00 | 1.94 | 20.9 |
| 1A1-10 | 161.2 | 135.3 | 194.4 | 1.19 | 0.83 | 305.0 | 0.77 | 234.9 | 0.28 | 1.94 | 18.7 |

| Specimen Id | Vexp (kN) | Vpred EC2 (kN) | Vpred Mari (kN) | Vexp/Vpred EC | Vexp/Vpred Mari | d (mm) | a/d | a (mm) | ρw (%) | ρl (%) | fck (MPa) |
|---|---|---|---|---|---|---|---|---|---|---|---|
| Smith & Vantsiotis, 1983 | | | | | | | | | | | |
| 1A3-11 | 148.3 | 135.3 | 183.2 | 1.10 | 0.81 | 305.0 | 0.77 | 234.9 | 0.28 | 1.94 | 18.0 |
| 1A4-12 | 141.2 | 135.3 | 174.1 | 1.04 | 0.81 | 305.0 | 0.77 | 234.9 | 0.28 | 1.94 | 16.1 |
| 1A4-51 | 170.9 | 138.2 | 205.2 | 1.24 | 0.83 | 305.0 | 0.77 | 234.9 | 0.28 | 1.94 | 20.5 |
| 1A6-37 | 184.1 | 139.4 | 216.3 | 1.32 | 0.85 | 305.0 | 0.77 | 234.9 | 0.28 | 1.94 | 21.1 |
| 0B0-49 | 149.0 | 104.0 | 143.2 | 1.43 | 1.04 | 305.0 | 1.01 | 308.1 | 0.00 | 1.94 | 21.7 |
| 1B1-01 | 147.5 | 104.6 | 164.2 | 1.41 | 0.90 | 305.0 | 1.01 | 308.1 | 0.24 | 1.94 | 22.1 |
| 1B3-29 | 143.6 | 101.4 | 159.0 | 1.42 | 0.90 | 305.0 | 1.01 | 308.1 | 0.24 | 1.94 | 20.1 |
| 1B4-30 | 140.3 | 102.6 | 158.0 | 1.37 | 0.89 | 305.0 | 1.01 | 308.1 | 0.24 | 1.94 | 20.8 |
| 1B6-31 | 153.4 | 100.4 | 164.2 | 1.53 | 0.93 | 305.0 | 1.01 | 308.1 | 0.24 | 1.94 | 19.5 |
| 2B1-05 | 129.0 | 149.9 | 164.5 | 0.86 | 0.78 | 305.0 | 1.01 | 308.1 | 0.41 | 1.94 | 19.2 |
| 2B3-06 | 131.2 | 149.9 | 165.6 | 0.88 | 0.79 | 305.0 | 1.01 | 308.1 | 0.41 | 1.94 | 19.0 |
| 2B4-07 | 126.1 | 149.9 | 160.0 | 0.84 | 0.79 | 305.0 | 1.01 | 308.1 | 0.41 | 1.94 | 17.5 |
| 2B4-52 | 149.9 | 149.9 | 181.5 | 1.00 | 0.83 | 305.0 | 1.01 | 308.1 | 0.41 | 1.94 | 21.8 |
| 2B6-32 | 145.2 | 149.9 | 175.5 | 0.97 | 0.83 | 305.0 | 1.01 | 308.1 | 0.41 | 1.94 | 19.8 |
| 3B1-08 | 130.8 | 224.9 | 179.4 | 0.58 | 0.73 | 305.0 | 1.01 | 308.1 | 0.62 | 1.94 | 16.2 |
| 3B1-36 | 159.0 | 276.8 | 216.7 | 0.57 | 0.73 | 305.0 | 1.01 | 308.1 | 0.76 | 1.94 | 20.4 |
| 3B3-33 | 158.4 | 276.8 | 214.1 | 0.57 | 0.74 | 305.0 | 1.01 | 308.1 | 0.76 | 1.94 | 19.0 |
| 3B4-34 | 155.0 | 276.8 | 212.4 | 0.56 | 0.73 | 305.0 | 1.01 | 308.1 | 0.76 | 1.94 | 19.2 |
| 3B6-35 | 166.1 | 276.8 | 221.6 | 0.60 | 0.75 | 305.0 | 1.01 | 308.1 | 0.76 | 1.94 | 20.6 |
| 0C0-50 | 115.7 | 68.8 | 97.3 | 1.68 | 1.19 | 305.0 | 1.34 | 408.7 | 0.00 | 1.94 | 20.7 |
| 1C1-14 | 119.0 | 67.2 | 121.5 | 1.77 | 0.98 | 305.0 | 1.34 | 408.7 | 0.18 | 1.94 | 19.2 |
| 1C3-02 | 123.4 | 70.1 | 126.8 | 1.76 | 0.97 | 305.0 | 1.34 | 408.7 | 0.18 | 1.94 | 21.9 |
| 1C4-15 | 131.0 | 70.9 | 131.4 | 1.85 | 1.00 | 305.0 | 1.34 | 408.7 | 0.18 | 1.94 | 22.7 |
| 1C6-16 | 122.3 | 70.0 | 126.1 | 1.75 | 0.97 | 305.0 | 1.34 | 408.7 | 0.18 | 1.94 | 21.8 |
| 2C1-17 | 124.1 | 75.6 | 142.9 | 1.64 | 0.87 | 305.0 | 1.34 | 408.7 | 0.31 | 1.94 | 19.9 |
| 2C3-03 | 103.6 | 75.6 | 132.2 | 1.37 | 0.78 | 305.0 | 1.34 | 408.7 | 0.31 | 1.94 | 19.2 |

| Specimen Id | Vexp (kN) | Vpred EC2 (kN) | Vpred Mari (kN) | Vexp/Vpred EC | Vexp/Vpred Mari | d (mm) | a/d | a (mm) | ρw (%) | ρl (%) | fck (MPa) |
|---|---|---|---|---|---|---|---|---|---|---|---|
| Smith & Vantsiotis, 1983 | | | | | | | | | | | |
| 2C3-27 | 115.3 | 75.6 | 137.9 | 1.53 | 0.84 | 305.0 | 1.34 | 408.7 | 0.31 | 1.94 | 19.3 |
| 2C4-18 | 124.6 | 75.6 | 143.8 | 1.65 | 0.87 | 305.0 | 1.34 | 408.7 | 0.31 | 1.94 | 20.4 |
| 2C6-19 | 124.1 | 75.6 | 144.0 | 1.64 | 0.86 | 305.0 | 1.34 | 408.7 | 0.31 | 1.94 | 20.8 |
| 3C1-20 | 140.8 | 134.4 | 185.5 | 1.05 | 0.76 | 305.0 | 1.34 | 408.7 | 0.55 | 1.94 | 21.0 |
| 3C3-21 | 125.0 | 134.4 | 171.7 | 0.93 | 0.73 | 305.0 | 1.34 | 408.7 | 0.55 | 1.94 | 16.5 |
| 3C4-22 | 127.7 | 134.4 | 175.4 | 0.95 | 0.73 | 305.0 | 1.34 | 408.7 | 0.55 | 1.94 | 18.3 |
| 3C6-23 | 137.2 | 134.4 | 181.1 | 1.02 | 0.76 | 305.0 | 1.34 | 408.7 | 0.55 | 1.94 | 19.0 |
| 4C1-24 | 146.6 | 186.1 | 215.4 | 0.79 | 0.68 | 305.0 | 1.34 | 408.7 | 0.76 | 1.94 | 19.6 |
| 4C3-04 | 128.6 | 151.2 | 185.7 | 0.85 | 0.69 | 305.0 | 1.34 | 408.7 | 0.62 | 1.94 | 18.5 |
| 4C3-28 | 152.4 | 186.1 | 217.7 | 0.82 | 0.70 | 305.0 | 1.34 | 408.7 | 0.76 | 1.94 | 19.2 |
| 4C4-25 | 152.6 | 186.1 | 216.7 | 0.82 | 0.70 | 305.0 | 1.34 | 408.7 | 0.76 | 1.94 | 18.5 |
| 4C6-26 | 159.5 | 186.1 | 223.9 | 0.86 | 0.71 | 305.0 | 1.34 | 408.7 | 0.76 | 1.94 | 21.2 |
| 0D0-47 | 73.4 | 40.5 | 55.0 | 1.81 | 1.34 | 305.0 | 2.01 | 613.1 | 0.00 | 1.94 | 19.5 |
| 4D1-13 | 87.4 | 86.9 | 150.7 | 1.01 | 0.58 | 305.0 | 2.01 | 613.1 | 0.41 | 1.94 | 16.1 |
| Vollum & Fang, 2014 | | | | | | | | | | | |
| B1-25 | 184.0 | 105.5 | 275.3 | 1.74 | 0.67 | 462.5 | 1.84 | 850.0 | 0.00 | 2.69 | 45.7 |
| B1-50 | 176.0 | 104.7 | 250.7 | 1.68 | 0.70 | 437.5 | 1.94 | 850.0 | 0.00 | 2.69 | 45.7 |
| B2-25 | 488.5 | 227.3 | 529.4 | 2.15 | 0.92 | 462.5 | 1.03 | 475.0 | 0.00 | 2.69 | 45.7 |
| B2-50 | 464.5 | 247.7 | 478.7 | 1.88 | 0.97 | 437.5 | 1.09 | 475.0 | 0.00 | 2.69 | 45.7 |
| A-2 | 174.5 | 123.8 | 176.7 | 1.41 | 0.99 | 442 | 1.92 | 850.0 | 0.00 | 2.69 | 35.6 |
| S1-2 | 300.5 | 260.7 | 419.8 | 1.15 | 0.72 | 442 | 1.92 | 850.0 | 0.30 | 2.69 | 35.6 |
| S2-2 | 410.0 | 260.7 | 437.9 | 1.57 | 0.94 | 442 | 1.92 | 850.0 | 0.42 | 2.69 | 35.6 |